From outcrop observations to dynamic simulations

an efficient workflow for generating ensembles of geologically plausible fracture networks and assessing their impact on flow and transport

Authors
Kamel Targhi, Elahe; Bruna, Pierre-Olivier; Daniilidis, Alexandros; Rongier, Guillaume; Geiger, Sebastian

DOI
10.1144/geoenergy2025-028

Publication date
2025

Document Version
Final published version

Published in
Geoenergy

Citation (APA)
Kamel Targhi, E., Bruna, P.-O., Daniilidis, A., Rongier, G., & Geiger, S. (2025). From outcrop observations to dynamic simulations: an efficient workflow for generating ensembles of geologically plausible fracture networks and assessing their impact on flow and transport. *Geoenergy*, *3*(1). https://doi.org/10.1144/geoenergy2025-028

Research article

Geoenergy

https://doi.org/10.1144/geoenergy2025-028 | Vol. 3 | 2025 | geoenergy2025-028

From outcrop observations to dynamic simulations: an efficient workflow for generating ensembles of geologically plausible fracture networks and assessing their impact on flow and transport

Elahe Kamel Targhi*, Pierre-Olivier Bruna, Alexandros Daniilidis, Guillaume Rongier and Sebastian Geiger

Department of Geoscience and Engineering, Delft University of Technology, Stevinweg 1, 2628CN Delft, The Netherlands
EK, 0000-0002-9931-6798; P-OB, 0000-0001-9403-8955; AD, 0000-0002-9063-4714; GR, 0000-0002-5910-6868; SG, 0000-0002-3792-1896
* Correspondence: e.kameltarghi@tudelft.nl

Abstract: Fractures are ubiquitous in geological formations and can often have an impact on subsurface applications such as geothermal energy, groundwater management or CO_2 storage. Quantifying the relationship between the uncertainties inherent to fracture networks and the corresponding flow behaviour for these applications remains an open challenge. Simulation studies that are based on outcrop analogues of fracture networks have yielded many new insights about heat and mass transfer in fractured geological formations but are restricted to a limited number of fracture network realizations, simplified assumptions about fracture network properties or deterministic models, making it difficult to analyse a wide range of uncertainties. This study introduces a flexible workflow that generates ensembles of geologically plausible fracture networks that can be based on statistical data from outcrop analogues. The fracture networks are generated using a computationally efficient approach that combines mechanical and statistical methods. The ensembles are then seamlessly linked to multi-purpose flow and transport simulations where the fractures are represented explicitly in a porous and permeable rock matrix. This approach can enable new uncertainty quantification methods, supported by machine-learning-based emulators, to analyse how fracture network properties, such as fracture intensity, fracture aperture or fracture orientation, influence heat and mass transfer in fractured geological formations. The workflow is illustrated using two classic example applications pertinent to fracture network modelling – one based on outcrop data to assess thermal behaviour in geothermal systems, and one synthetic study to analyse the transition from matrix-dominated to fracture-dominated flow – and released as open-source code.

Thematic collection: This article is part of the sustainable future of geoenergy in the hands of early career researchers collection available at: https://www.lyellcollection.org/content/geoenergy-early-career-research

Received 16 June 2025; **revised** 14 August 2025; **accepted** 20 August 2025

Naturally occurring fractures are ubiquitous in the subsurface (cf. Berkowitz 2002; Viswanathan *et al*. 2022). It is well understood that these fractures can form high-permeability zones that significantly influence heat and mass transfer in geological formations, affecting the exploitation of geothermal resources (e.g. Vidal *et al*. 2017), groundwater management and remediation (e.g. Medici *et al*. 2021), reactive transport in karst systems (e.g. Andre and Rajaram 2005), radioactive waste disposal (e.g. Tsang *et al*. 2015) or CO_2 storage (e.g. March *et al*. 2018).

For many years, outcrop analogues have been used to simulate heat and mass transfer through geologically plausible fracture networks (Geiger and Matthäi 2014). These models are based on explicit representations of the fractures; that is, fractures are represented in the models as they have been observed in an outcrop while bespoke numerical simulation techniques are used to model flow and transport processes in the fully resolved fracture network and the permeable rock matrix (cf. Berre *et al*. 2019). This approach has yielded fundamentally new insights into how the structure of fracture networks, the matrix properties and the fracture–matrix interactions affect the dispersion of solutes (Geiger *et al*. 2010; Edery *et al*. 2016) and heat (Geiger and Emmanuel 2010; de Hoop *et al*. 2022) in fractured geological formations. It has also been used to examine how multiphase flow processes, for example related to CO_2 storage, are influenced by fractures and can be upscaled (Gierzynski and Pollyea 2017; Rizzo *et al*. 2024). Additionally, several studies have investigated how fracture connectivity, topology and aperture models have an impact on the effective fracture–matrix permeability and fracture–matrix interactions (Matthäi and Belayneh 2004; Hardebol *et al*. 2015; Bisdom *et al*. 2016*b*; Sævik and Nixon 2017), as well as how geomechanical processes affect flow and transport in fractured geological formations (Lei *et al*. 2015, 2017; Kang *et al*. 2019).

One fundamental shortcoming of such outcrop-based simulation studies of heat and mass transfer in fractured porous media is that they are based on deterministic models, i.e. simulations are always based on a small number of fracture patterns observed in outcrops. Consequently, with this approach it is difficult to quantify how uncertainties inherent to subsurface fracture networks affect flow and transport behaviour. Subsequently, it is also not possible to utilize a large number of simulation results carried out for a wide range of outcrop-informed fracture networks to train machine-learning approaches to quantify such uncertainties. Yet, Viswanathan *et al*. (2022) have identified the development of 'physics-based models with machine-learning emulators [to] enable uncertainty quantification of flow and transport in complex fracture networks' as a key research challenge for fractured reservoirs. Recent studies have demonstrated that, in principle, machine learning can be a powerful approach to classifying fracture-matrix interactions (Andrianov and Nick 2021; Ashworth *et al*. 2022) or connecting fracture network properties to pressure transient signals observed at wells (Freites *et al*. 2023). However, these studies are still based on idealized fracture geometries that do not capture the

inherent complexity and multiscale nature of fracture networks observed in outcrops.

Two requirements must be met to generate training data for machine-learning-based uncertainty quantification using geologically plausible fracture networks that reflect key outcrop characteristics. First, numerically efficient ways to generate a sufficiently large ensemble of fracture networks are needed. Second, the ensemble of fracture networks needs to be utilized in a straightforward manner in multi-purpose flow and transport simulations where each fracture can be represented explicitly in a permeable and porous matrix. In the following, we provide a brief summary of how fracture networks can be generated. We will also summarize how heat and mass transfer can be simulated using explicit methods.

Three methods exist to generate fracture networks where fractures are represented explicitly: mechanical, statistical and hybrid approaches, each with its distinct advantages and disadvantages (Welch *et al.* 2020). The statistical approach aims to generate fracture networks that honour the statistical properties of fracture data observed in the subsurface (Dershowitz 1984; Wenli *et al.* 2019). A fracture network is generated based on the observed distributions for fracture length, fracture orientation and sometimes fracture spacing (Hope *et al.* 2015; Berrone *et al.* 2018; Agbaje *et al.* 2023; Lavoine *et al.* 2023). The main drawback of this approach is that mechanical processes that constrain the placement of fractures within the network are not considered. This can result in fracture networks where connectivity, permeability and flow processes differ significantly from fracture networks that are generated with mechanical constraints (Maillot *et al.* 2016). In addition, the random arrangement of fractures within these networks contradicts the well-organized fracture patterns observed in outcrop exposures. Although attempts exist to incorporate geological rules that create fracture networks with more geological consistency, these methods are often computationally inefficient, particularly when dealing with networks with a large number of fractures (Boersma 2020).

The mechanical approach is based on simulating the growth of fractures by modelling the propagation and interaction between individual fractures and the rock matrix (e.g. Paluszny *et al.* 2020; Thomas *et al.* 2020; Zimmerman and Paluszny 2023; Pezzulli *et al.* 2025). This approach consists of three steps: nucleation, growth and arrest of fractures (Davy *et al.* 2013, 2014; Welch *et al.* 2020). The main drawback of the mechanical approach is its high computational cost, which renders the generation of an ensemble of fracture networks, where each network contains hundreds or thousands of individual fractures, intractable (Olson 1997; Olson *et al.* 2001; Welch *et al.* 2020).

The hybrid approach aims to combine the advantages of the statistical and mechanical approaches (Srivastava *et al.* 2005; Bonneau *et al.* 2013). For example, Bonneau *et al.* (2013) proposed to integrate fracture growth and fracture statistics to create geomechanically consistent fracture networks by simulating mechanical interactions between fractures. However, their proposed workflow results in fracture networks that do not fully match the input statistics, meaning their statistical properties may differ from the original input data. Additionally, this particular workflow is still not computationally efficient enough to generate ensembles of fracture networks.

Flow and transport modelling approaches that represent fractures explicitly fall into two classes, the discrete fracture matrix (DFM) and discrete fracture network (DFN) models (Karimi-Fard *et al.* 2006; Rogers *et al.* 2007). The main difference between these two approaches lies in the way the rock matrix is represented (cf. Berre *et al.* 2019): the DFM approach considers the matrix as a porous and permeable medium, allowing for fluid flow in both fractures and rock matrix. The DFN model treats the matrix as an impermeable and non-porous medium, so fluid flow occurs only within the fracture network. Several numerical approaches have been developed for simulating fluid flow using DFM and DFN models. These approaches include, but are not limited to, Embedded Discrete Fracture Modelling (EDFM) (e.g. Lee *et al.* 2001; Li and Lee 2008; Fumagalli *et al.* 2016; Ţene *et al.* 2017), the finite volume method that utilizes unstructured grids (e.g. Karimi-Fard *et al.* 2006; Reichenberger *et al.* 2006; Namdari *et al.* 2021), the extended finite element method (e.g. Flemisch *et al.* 2016) or methods combining finite element and finite volume methods (e.g. Nick and Matthäi 2011; Flemisch *et al.* 2018).

Recently, the first workflows have been proposed to link fracture networks observed in outcrops to geothermal flow simulations to analyse how uncertainties in fracture data could affect predictions in heat flow modelling (Lepillier *et al.* 2019, 2020). However, these workflows are still limited when representing the geometric complexities that are encountered in fracture networks and can only use a limited range of input data. Similarly, workflows have been introduced that link fracture networks observed in outcrops to mechanical models to analyse how fracture aperture variations affect fluid flow (Bisdom *et al.* 2017*b*). Workflows also exist to estimate the fracture network permeability directly from the fracture patterns observed in outcrops (Healy *et al.* 2017). However, these workflows are still using deterministic fracture models and therefore do not yet allow uncertainty quantification via ensembles of fracture networks (Rutqvist *et al.* 2013). There is a need to develop a flexible approach that allows us to use a broad range of statistical input parameters observed in outcrops to generate geologically plausible fracture networks in a computationally efficient way and deploy the resulting ensemble of fracture networks in multi-purpose flow simulations to address a wide range of subsurface flow problems. Such an approach would then pave the way for the development of new methods that facilitate machine-learning enabled uncertainty quantification techniques for fractured geological formations (Viswanathan *et al.* 2022).

In this paper we aim to address this gap by developing a flexible and efficient approach that links outcrop observations of fracture networks to flow modelling using DFM methods. First, we introduce a workflow that integrates mechanical and statistical methodologies to generate DFNs, explicitly considering stress shadows around fractures (Davy *et al.* 2013; Welch *et al.* 2020). Incorporating stress shadows enables realistic fracture configurations without resorting to computationally expensive fracture growth simulations. This approach enables the generation of ensembles of geologically plausible fracture networks, allowing exploration of uncertainties in fracture properties derived from statistical analyses of outcrop data. The workflow is then linked directly to a reservoir simulator, which enables efficient numerical simulations to evaluate how these uncertainties affect fluid flow processes, including heat and mass transfer within both the fracture network and the permeable rock matrix. Our integrated approach is provided through an open-source software tool, GeoDFN, written in Python, that is directly connected to the open-source Matlab Reservoir Simulation Toolbox (MRST) (Lie *et al.* 2012; Lie 2019) to facilitate a broad range of subsurface flow simulations in fractured geological formations, including but not limited to aquifer management (Li *et al.* 2020; Masciopinto *et al.* 2021), solute transport (Tran and Jha 2021), upscaling in fracture networks (Fumagalli *et al.* 2016; Wong *et al.* 2020) or enhanced geothermal systems (Zhang *et al.* 2024).

This paper is structured as follows: In the section ‘Overview of fracture growth mechanics, fracture aperture models and fracture statistics’, we provide a brief summary of the key fracture modelling concepts, including the physics of fracture growth and models to approximate fracture apertures. We also summarize the statistics used to represent the fracture properties (i.e. orientation, length and spacing) in a given fracture network. In the section ‘Integrated workflow’, we

outline the workflow to generate geologically plausible fracture networks from outcrop observations and explain how these networks can be used in flow simulations. In the section 'Application examples', we illustrate this workflow by applying it to two classic flow modelling problems in fractured porous media. Finally, in the conclusions, we summarize the contributions of this work.

Overview of fracture growth mechanics, fracture aperture models and fracture statistics

Physics of fracture growth

Fractures initiate at rock flaws when the net energy released by fracture growth is positive (Griffith 1921; Pollard and Aydin 1988). Fracture growth and propagation continues as long as some energy is available, which is influenced by the stress field (Atkinson 1982; Atkinson and Craster 1995; Pezzulli *et al*. 2025). The termination of fractures can also occur when the fracture tip enters the stress shadow of an existing fracture. The stress shadow is a region around a fracture where the local stress field is altered due to the presence of the fracture. Within the stress shadow, fractures are less likely to grow or initiate because the available energy for fracture propagation is lower (Nur 1982; Bonneau *et al*. 2013; Davy *et al*. 2013; Welch *et al*. 2020). In the framework of modelling fracture networks using the fracture growth principle, Welch *et al*. (2019) conceptualized the stress shadow as a rectangular zone around fractures, referred to as the buffer zone. The width of the stress shadow is generally proportional to the minimum dimension of the fracture, which, for layer-bound fractures, is typically assumed to be the layer height (Welch *et al*. 2019). However, Bonneau *et al*. (2013) suggested that the width of a stress shadow is between 10 and 50% of the corresponding fracture length because larger fractures have greater distances between them and neighbouring fractures (Masihi and King 2007).

The stress shadow is an important concept in fracture modelling because it imposes a minimum spacing between fractures, affecting network configuration and connectivity (Bai *et al*. 2000, 2002). For example, Bai and Pollard (2000*b*) demonstrated that, as the spacing between Mode I fractures continues to decrease, the fractures reach such a close spacing that, even with increasing strain, no new fractures can initiate in the network and the propagation of existing fractures stops. This phenomenon is referred to as fracture saturation (Bai and Pollard 2000*b*). Below we will discuss how fracture saturation can be used as a criterion to detect if input parameters for generating fracture networks are consistent.

Fracture aperture modelling

Fracture aperture is one of the key properties influencing the permeability of fractures, hence affecting flow and transport in the entire network (e.g. Lei *et al*. 2015, 2017; Bisdom *et al*. 2017*a*; Kang *et al*. 2019). The permeability of an individual fracture, k, can be estimated as a function of fracture aperture, α, using the parallel-plate model (Snow 1968) as

$$k = \frac{\alpha^2}{12} \tag{1}$$

This first-order model provides high accuracy for fractures with locally uniform apertures, and it can be extended to incorporate effects such as surface roughness and contact area (Denetto and Kamp 2016; Zimmerman and Paluszny 2023). A common simplification in outcrop-based simulation studies assumes a constant aperture across all fractures in the network (e.g. Min *et al*. 2004; Geiger and Emmanuel 2010; Geiger *et al*. 2010; Hardebol *et al*. 2015). However, several studies that consider fractures at different scales, from laboratory to outcrop scale, indicate that apertures vary markedly among different fractures (Laubach and Ward 2006; Iñigo *et al*. 2012; Hooker *et al*. 2013). Such variability in fracture aperture can be modelled using different empirical relationships (Vermilye and Scholz 1995; Marrett *et al*. 1999; Hooker *et al*. 2014). Here, we discuss the three most commonly used relationships for approximating fracture apertures in a fracture network.

Olson (2003) proposed a sub-linear scaling relationship that relates fracture aperture to fracture length that is based on fracture propagation criteria in a linear elastic fracture mechanics framework. This relationship is given by

$$\alpha = CL^{\beta} \tag{2}$$

where C is a pre-exponential constant that depends on the fracture toughness and elastic properties of the host rock (refer to Olson (2003) for further details of how to calculate C), and β is an exponent indicating the degree of (non-)linearity in the relationship between fracture length and aperture. This approach assumes that fractures of different lengths in a homogeneous rock matrix share a uniform stress intensity factor.

Lepillier *et al*. (2019) relaxed the assumption of stress uniformity and suggested that stress intensity varies with fracture orientation and length. The deformation of the fracture aperture due to an existing stress field is calculated using Hooke's law as

$$\Delta\alpha = \sigma_{\mathrm{n}}/K_{\mathrm{n}} \tag{3}$$

where σ_{n} is the normal stress, which varies for each fracture depending on its orientation to the stress field, and K_{n} is the normal stiffness. K_{n} is calculated using

$$K_{\mathrm{n}} = \frac{E(1-\nu)}{\alpha_{\mathrm{a}}(1+\nu)(1-2\nu)} \tag{4}$$

where α_{a} is the fracture aperture observed in the outcrop, E is the Young's modulus and ν is the Poisson's ratio (Lepillier *et al*. 2019). This method can be used to calculate the fracture aperture in the subsurface based on the apparent aperture observed in the outcrop. However, since the aperture observed in outcrops is often altered by weathering, the calculation may be based on inaccurate input data.

The Barton–Bandis model (Barton *et al*. 1985) is an empirical approach that quantifies the residual fracture aperture, i.e. the fracture aperture that remains when irregular fracture walls are partially closed under compression. The Barton–Bandis model approximates the stress-dependent fracture aperture as

$$\alpha = \alpha_0 - \left(\frac{1}{V_{\mathrm{m}}} + \frac{K_{\mathrm{ni}}}{\sigma_{\mathrm{n}}}\right)^{-1} \tag{5}$$

where α_0 represents the initial aperture, V_{m} is the maximum closure, and K_{ni} is the initial normal stiffness. These parameters are dependent on the Joint Roughness Coefficient (JRC) and the Joint Wall Compressive Strength (JCS). A detailed description of how to calculate these parameters, and the limitation of them, is provided in Bisdom *et al*. (2016*a*).

Bisdom *et al*. (2016*b*) analysed how these different approaches for estimating fracture aperture affect the overall fracture network permeability, as well as the effective permeability of the fracture network and matrix together. Their findings suggest that linear length-aperture scaling typically results in the largest apertures, while the Barton–Bandis model produces smaller apertures. They demonstrated that the Barton–Bandis model predicts higher permeability when the rock matrix has low permeability due to a greater proportion of critically stressed fractures, whereas linear length-aperture scaling leads to higher permeability if the rock matrix has high permeability. Overall, the work by Bisdom *et al*. (2016*b*) highlights that fracture aperture models are a key uncertainty when modelling flow and transport processes in

fractured geological formations. Hence, this uncertainty should be included when generating ensembles of fracture networks for uncertainty quantification studies.

Statistical representation of fractures in a fracture network

When generating fracture networks statistically, the properties of each fracture (i.e. length, orientation and spacing) are determined by sampling from a given probability distribution function (PDF). Selecting the appropriate PDF for a given fracture network property (e.g. length) is crucial because the PDF affects the connectivity of the modelled network and, consequently, properties such as the overall permeability of the fracture network (de Dreuzy *et al.* 2001, 2004). In this section, we briefly review the most commonly used PDFs to characterize fracture network properties (Table 1).

Power-law distributions for fracture length are commonly used, based on abundant data from outcrop and experimental studies (Hooker *et al.* 2014; Sun *et al.* 2016; Welch *et al.* 2019; Agbaje *et al.* 2023; Lavoine *et al.* 2023). Alternatively, Olson *et al.* (2001) suggested an exponential distribution while Gutierrez and Youn (2015) suggested a log-normal distribution. The PDFs describing fracture lengths can be directly linked to the underlying mechanisms of fracture growth. Power-law distributions are typically associated with scale-invariant growth where longer fractures grow faster, log-normal distributions with externally constrained or semi-regular growth, and exponential distributions with random, memoryless processes (Bonnet *et al.* 2001; Davy *et al.* 2013).

The spatial distribution of fractures, which is related to the location of each individual fracture, is also influenced by the fracture propagation rate. Slow sub-critical propagation results in random spacing, intermediate rates yield regularly spaced fractures and fast rates lead to fractal, power-law distributions (Olson *et al.* 2001; Olson 2004). Hooker *et al.* (2014) observed this behaviour in the spatial distribution of fractures in outcrop data, ranging from regular to irregular spacing. Gillespie *et al.* (1993) noted that fracture spacing ranges from clustered, especially near faults, to more evenly distributed. Building on these studies, random, Poisson and log-normal distributions are frequently used in fracture network modelling approaches (Davy *et al.* 2013; Gutierrez and Youn 2015; Hope *et al.* 2015; Sun *et al.* 2016; Freites *et al.* 2023). As mentioned above, the concept of a stress shadow around individual fractures aims to generate fracture networks that are geologically more plausible. However, the presence of a stress shadow also defines a minimum distance between two adjacent fractures, which can influence the spatial distribution of fractures (Bai and Pollard 2000*a*; Bai *et al.* 2000). This aspect will be discussed further below.

Fracture orientation in geological formations is determined by the prevailing stress conditions during fracture formation. Distribution functions for fracture orientation typically reflect how fracture patterns vary as a function of scale (Darcel *et al.* 2009). The Fisher distribution is frequently used to model fracture orientations because it can represent various types of data (e.g. outcrop or borehole image data) with only three parameters (Dershowitz and Herda 1992; Alain and Vincent 2004; Huang *et al.* 2020; Zhang *et al.* 2021; Agbaje *et al.* 2023). When modelling fractures in 2D, the von Mises distribution is often used (Fadakar Alghalandis *et al.* 2011; Hope *et al.* 2015; Lavoine *et al.* 2023). The von Mises distribution is symmetrical and unimodal and hence suitable for circular data (Tran 2007). In some cases, constant and uniform distributions are also considered for assigning fracture orientation (Boersma 2020).

Integrated workflow: from outcrops to fracture network generation and flow modelling

Outcrop data are typically collected from lower-dimensional horizontal pavements or vertical cliff faces, both of which have limited exposure (cf. Zeeb *et al.* 2013; Healy *et al.* 2017). In sedimentary formations, fractures are also often subvertical and terminate at interfaces between different lithologies, i.e. are bed-confined (e.g. Narr and Suppe 1991; Narr *et al.* 2006). Consequently, as a first approximation, studies that analyse heat flow, contaminant transport and CO_2 storage in outcrop-derived fracture networks are often two-dimensional as well (e.g. Odling and Roden 1997; Geiger and Emmanuel 2010; Edery *et al.* 2016; Gierzynski and Pollyea 2017; de Hoop *et al.* 2022). Restricting outcrop-based simulation studies for heat and mass transfer in fractured geological formations to two dimensions also has the added advantage that computational requirements are tractable, which is key to uncertainty quantification workflows and generating training data for machine-learning. We therefore demonstrate a 2D workflow as well but note that the approach can be extended to 3D without loss of generality.

Once fracture data have been collected using drone imagery, LiDAR data or other means of image analysis or mapping (e.g. Bellian *et al.* 2005; Zeeb *et al.* 2013; Watkins *et al.* 2015; Bisdom *et al.* 2017*b*), the statistical properties of the fracture network need to be quantified to identify the PDFs (Table 1) that best represent the observed data. Using the chosen PDFs, we then pursue a hybrid approach to generate an ensemble of fracture networks that represent the outcrop data. This approach involves the following three steps (Fig. 1).

First, we generate a dataset of fractures by sampling their lengths and orientations from the PDFs that have been identified. Note that we consider a wide range of PDFs (Table 1) to provide as much flexibility as possible when representing the characteristics of fracture length, orientation and spacing observed in the outcrop.

Table 1. PDFs for representing fracture network statistics in terms of length, spacing and orientation

Name	Equation		Length	Spacing	Orientation
Log-normal	$f(x) = \frac{1}{x\sigma\sqrt{2\pi}}\exp\left[-\frac{(\ln x-\mu)^2}{2\sigma^2}\right]$	(6)	*	**	–
Power-law	$f(x) = x^{-n}$	(7)	***	**	–
Exponential	$f(x) = \lambda e^{-\lambda x}$	(8)	**	–	–
von Mises	$f(x) = \frac{e^{\kappa\cos(x-\mu)}}{2\pi I_0(\kappa)}$	(9)	–	–	***
Constant	$f(x) = c$	(10)	*	–	*
Uniform (random)	$f(x) = \frac{1}{b-a}$	(11)	–	***	**

Notes: In the log-normal distribution, μ and σ are the mean and standard deviation, and ln represents the natural logarithm. n is the exponent in the power-law distribution, and λ is the rate parameter for the exponential distribution. In the von Mises distribution, μ is the mean direction, and κ is the concentration parameter. c is a constant value in the constant distribution, and a and b are the minimum and maximum values for the uniform distribution.The number of asterisks indicates how commonly a function is used for a given property (–, not applicable; *, rarely used; **, moderately used; ***, commonly used).

Fig. 1. Schematic diagram illustrating the individual steps for generating and placing the fractures for each fracture set.

These PDFs are normally truncated to only include the ranges observed in the outcrop. It is often possible to represent the same outcrop data reasonably well with different PDFs. Since each PDF leads to a variation in fracture network configurations, ranging from more clustered patterns in log-normal and power-law distributions to more uniform patterns (Fig. 2a), we can create ensembles of fracture networks that also account for uncertainties in how the raw fracture data are interpreted and modelled.

Second, the longest fracture of a given fracture set is inserted into the model domain. Starting the generation of a fracture network by placing the longest fracture is motivated by the observation that longer fractures grow first and reach their full extent before shorter fractures begin to propagate (Olson 2007; Bonneau *et al.* 2013). Normally, a random location is selected for the longest fracture. This location is chosen to ensure that the entire fracture lies within the domain boundaries, which prevents the need to truncate fractures that would extend beyond the model boundary otherwise. The random nature of placing the first fracture allows us to generate an ensemble of equiprobable fracture networks because, for each new fracture network, all subsequent fractures are positioned relative to the longest fracture.

Third, the remaining fractures of a given fracture set are placed sequentially, starting with the second longest fracture and progressing to the shortest fracture. Fractures are placed relative to the longest fracture. The distance between each newly placed fracture and the longest fracture in the set is determined by the PDF that was chosen to quantify the spatial distribution. When placing a new fracture, two criteria are considered. First, a coordinate check is carried out to ensure the fracture lies within the bounds of the domain. Second, a proximity check is carried out to ensure that the new fracture and its stress shadow do not intersect with an existing fracture and its stress shadow from the same set (Fig. 3). The stress shadow is represented by a rectangular buffer zone around each fracture. Depending on the outcrop observations, this buffer zone is set to either have a constant width for all fractures (Welch *et al.* 2019) or its width scales linearly with the fracture length (Bonneau *et al.* 2013). New fractures are placed until the target areal fracture intensity P_{21} is reached, which indicates that all sampled fractures have been successfully placed within the domain (Dershowitz and Herda 1992). We define P_{21} as

$$P_{21} = \frac{\sum_{n}^{i=1} l_i}{A} \tag{12}$$

where l_i is the length of the ith fracture, and n is the total number of fractures that exist within the area of A. The second and third steps are repeated for all fracture sets, resulting in an ensemble of equiprobable fracture networks.

In a post-processing operation, the fracture aperture is calculated for each fracture in the network using one of four options: a constant fracture aperture, a sub-linear length-aperture correlation (equation 2), the method of Lepillier *et al.* (2019) (equations 3, 4) or the Barton–Bandis model for a given far-field stress (equation 5). These fracture aperture models allow us to further expand the ensemble of

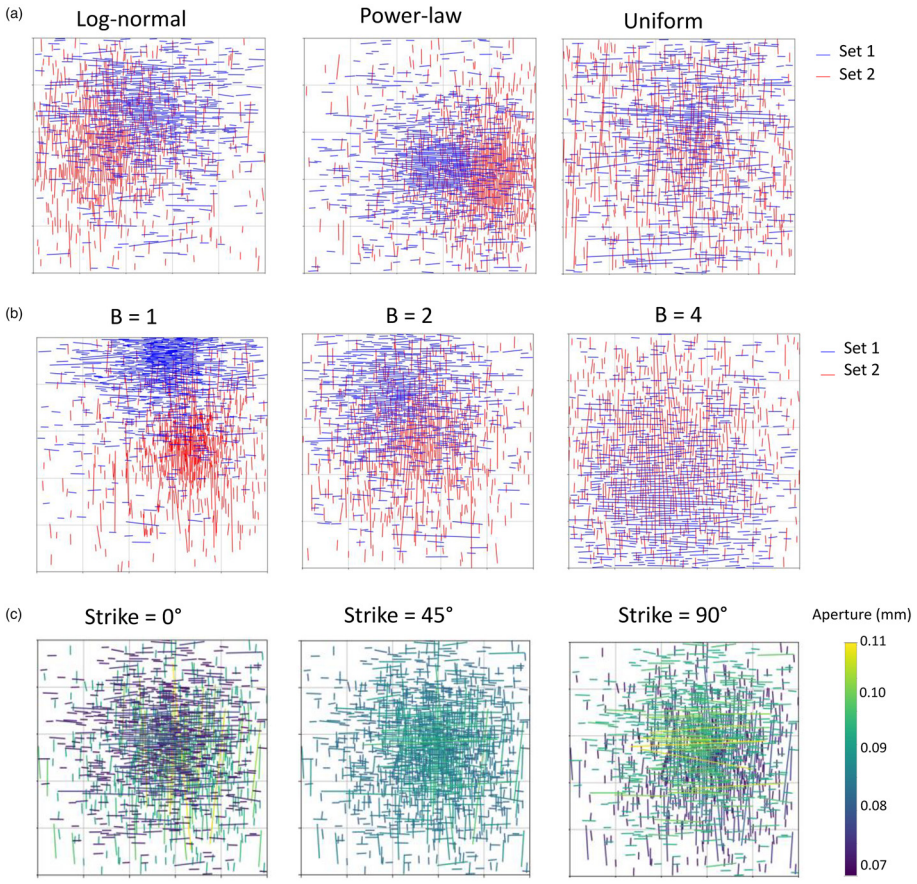

Fig. 2. Illustrative examples that show (**a**) the effect of different PDFs and (**b**) the influence of the buffer zone width B on the fracture network geometries, as well as (**c**) the impact of stress orientation on fracture aperture distributions. Red and blue colours denote different fracture sets in (a) and (b). Input parameters for generating these fracture networks are given in Tables A1 and A2 in the Appendix.

fracture networks by accounting for uncertainties in fracture permeability, which, as discussed above, is a major uncertainty affecting heat and mass transfer in fractured geological formations. Figure 2c is an example that illustrates how fracture apertures change in just one fracture network if the stress tensor is rotated in the Barton–Bandis model.

On a standard laptop, generating a single fracture network requires between 30 seconds and 20 minutes depending on the domain size and target P_{21} fracture intensity. Each generated fracture network is saved for visualization and to provide the geometry for subsequent numerical simulations.

Here we use MRST (Lie *et al.* 2012; Lie 2019) because it is an open-source software that has been widely applied to simulate a wide range of flow and transport processes in fractured geological formations (Fumagalli *et al.* 2016; Li *et al.* 2020; Wong *et al.* 2020; Masciopinto *et al.* 2021; Tran and Jha 2021; Zhang *et al.* 2024). Although MRST has the option to perform simulations in fractured geological formations using implicit methods (March *et al.* 2021), we specifically use the EDFM approach in MRST. In EDFM, the matrix grid and the fracture grid are generated independently, allowing fractures to be represented explicitly without requiring a complex, computationally expensive conforming mesh. Fracture–matrix and fracture–fracture flow are captured using non-neighbouring connection, which are transmissibility-based links between intersecting cells (Lee *et al.* 2001; Li and Lee 2008; Wong *et al.* 2021). We note that while we use MRST here, flow and transport modelling can also be carried out with other multi-physics open-source codes that can represent fracture networks using explicit methods such as Dumux (Flemisch *et al.* 2011), DARTS (Voskov *et al.* 2024), PorePy (Keilegavlen *et al.* 2021) or OpenCSMP (Matthai 2024).

This integrated approach provides significant flexibility to generate ensembles of fracture networks that allow us to explore how uncertainties in data and uncertainties in interpreting data affect flow and transport behaviour. However, there are two important aspects to consider. First, an increase in the width of the buffer zone leads to increasingly less clustering in the fracture networks (Fig. 2b). This means that log-normal and power-law PDFs that yield fracture networks that naturally exhibit clustering of

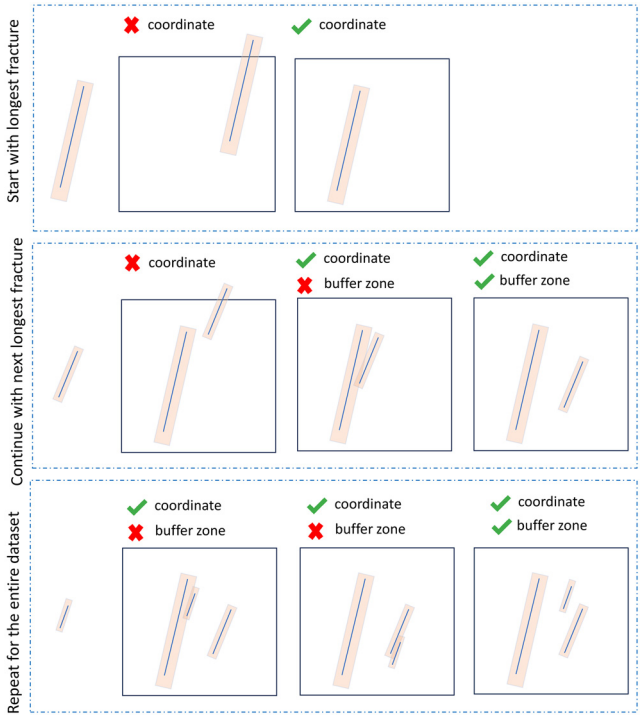

Fig. 3. Schematic diagram illustrating the placement of a new fracture. Fractures are indicated by blue lines and shadow zones by the rectangular shaded area around them.

fractures (Fig. 2a) can also yield fracture networks with limited or no clustering.

Secondly, it is possible to select combinations of PDFs and other input parameters, most notably the areal fracture intensity P_{21}, that are not consistent with each other. If P_{21} is chosen to be high, especially if the width of the buffer zone is also high, then situations can occur where there is insufficient space to add further fractures to the network, i.e. fracture saturation is reached (Fig. 4). In these instances, the generated fracture network would have different statistics from the input data and needs to be discarded. In other words, if fracture saturation has been reached before the target P_{21} can be obtained for the fracture network, the combination of input parameters and PDFs is likely not consistent and non-physical.

We note, however, that both of these aspects are common to many geostatistical methods (Bai and Pollard 2000*a*; Bai *et al.* 2000). They simply imply that any input data that are being used have to be consistent with the geology that one aims to model.

We further note that in the proposed workflow we do not attempt to reproduce observed fracture connectivity (e.g. the proportions of I, Y and X nodes). Instead, connectivity emerges from the placement rules. Further development could include calibrating ensembles against simple topological descriptors of connectivity derived from outcrop data, which would help align network topology with observations while preserving the statistical constraints. Moreover, although the current implementation is designed for naturally fractured networks, the framework could be extended to hydraulic fractures if reliable statistics on length, spacing and orientation are available. Such an extension would also require additional physics, notably coupling between pressure, stress and aperture during flow.

Application examples

In this section we present two examples to illustrate how the proposed workflow can be applied. In the first example, we show how fracture networks can be created based on the statistics observed in an outcrop analogue. We then perform geothermal heat flow simulations for these networks and compare them to the performance of the fracture network observed in the outcrop (Geiger and Emmanuel 2010; de Hoop *et al.* 2022). In the second example, we revisit the much-studied problem of when fracture networks become connected so that the flow behaviour transitions from a single-continuum system, where the fractures enhance the matrix permeability, to a dual-continua system, where the fractures dominate permeability and the matrix only provides storage for fluids and heat (Bogdanov *et al.* 2003; Sævik *et al.* 2014; Wong *et al.* 2020; Agbaje *et al.* 2023; He *et al.* 2023). Understanding this transition of flow regimes is critical not only for many subsurface applications in fractured geological formations but also for determining how to best represent fractures in simulation models (cf. Berre *et al.* 2019). As noted previously, MRST is a multi-purpose simulator, so these examples are only of an illustrative nature, and other applications such as CO_2 storage, heat flow or solute transport could also be readily studied using the proposed workflow.

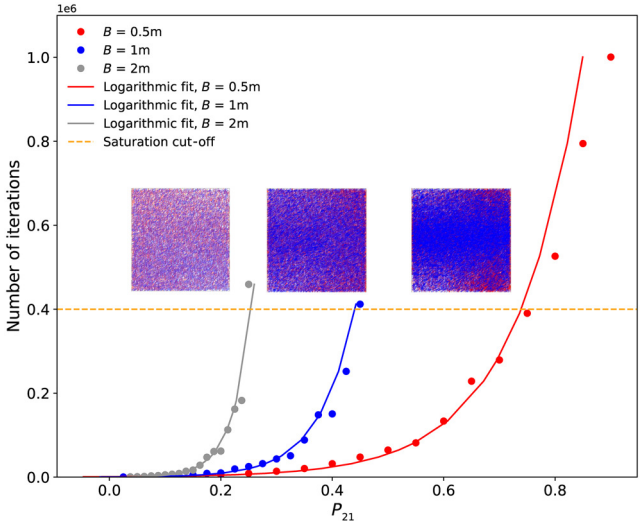

Fig. 4. Relationship between areal fracture intensity P_{21} and the number of iterations required when generating the fracture network for different buffer zone widths B. The dashed yellow line indicates fracture saturation, i.e. the point at which no further fractures can be placed in the network for the given domain size and value of B. If the target P_{21} is larger than the P_{21} at which fracture saturation has been reached, then the statistics of the generated fracture network do not match the input statistics. In this case, the network is discarded because the chosen input data are inconsistent. The fracture networks illustrate the fracture geometries at the point when fracture saturation is reached for the different B values. Red and blue colours indicate the two different fracture sets.

Outcrop-based fracture network modelling and effective comparative analysis of thermal behaviour

Geological data

We use the raw fracture data from the Apodi outcrop in the Jandaíra Formation, located in NE Brazil in the state of Rio Grande do Norte within the Potiguar Basin. This carbonate outcrop is a well-exposed pavement from which fractures can be readily mapped using drone imagery (Bisdom *et al.* 2017*a*). A total of 715 fractures have been mapped in the outcrop across an area of 120 000 m^2 (Fig. 5). The NE and SW parts of the Apodi outcrop are partially covered by vegetation. Three fracture sets were identified with east–west, NW–SE and north–south orientations, respectively (Fig. 5). The fractures exhibit clustering in an east–west direction (Set 1) and partially in a north–south direction (Set 2).

Fracture network modelling

The statistical parameters required for generating the fracture networks were obtained by matching the available distribution functions (Table 1) to the raw data for fracture orientation, spacing and length observed at the Apodi outcrop (Table 2). The raw data were collected by Bisdom *et al.* (2017*a*). We used the SciPy library to identify the distribution functions that match these data best (Virtanen *et al.* 2020). Values for P_{21} and buffer zone width were taken directly from the outcrop data.

As noted above, the fracture networks in the outcrop display certain characteristics, namely clustering of fractures in Set 1 and partially in Set 2. Furthermore, parts of the outcrop are covered by vegetation. This implies that if a rectangular domain is taken to generate the fracture networks, which is the most common approach, the area where fractures are observed is different from the area where fractures are modelled and hence inconsistencies may occur when generating the fracture networks. For these reasons, we consider three different scenarios when generating fracture networks.

(1) Scenario A. We use the default approach and place fractures randomly in a rectangular domain, i.e. ignore the fact that two fracture sets exhibit clustering in specific locations and that the domain where fractures have been mapped is partially covered by vegetation.
(2) Scenario B. We place the first fractures for Sets 1 and 2 in the areas where clustering is observed to ensure that the fractures are generated where they are observed in the

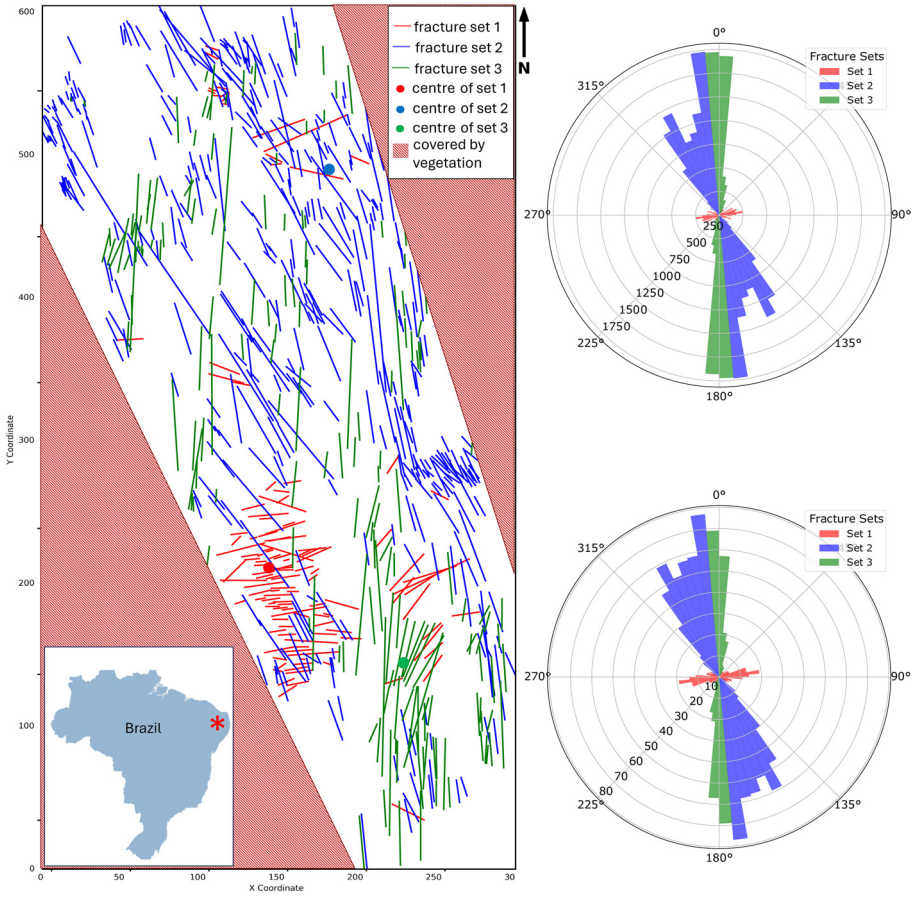

Fig. 5. Map of the Apodi outcrop indicating the fractures. Areas covered by vegetation are indicated in red. Each fracture set is displayed in a different colour. Dots indicate the approximate centre of each fracture set. Rose plots show the frequency-weighted (top) and length-weighted (bottom) fracture orientations. The inset shows the approximate location of the Apodi outcrop in the NE of Brazil (State of Rio Grande do Norte).

outcrop but still ignore the fact that part of the outcrop is covered by vegetation.

(3) Scenario C. As in Scenario B, we place the fractures in the regions where clustering is observed but now do not place any fractures in the areas that are covered by vegetation to ensure that the domains where fractures are observed and fractures are modelled are consistent with each other.

Table 2. Fracture statistics for the Apodi outcrop (domain size 300 × 600 m^2)

Parameter	Set 1	Set 2	Set 3
Fracture intensity			
P_{21} (m^{-1})	0.01	0.0435	0.0256
Fracture length			
Distribution	log-normal	log-normal	log-normal
μ (m)	2.344	2.733	3.0617
σ	0.73	0.68	0.66
Minimum length (m)	2.59	2.23	1.2
Maximum length (m)	57.48	114.92	121.62
Fracture orientation			
Distribution	von Mises	von Mises	von Mises
κ	8.55	24.5	58.16
μ (radian)	1.4	2.75	0.063
Minimum orientation (degree)	30	120	-5
Maximum orientation (degree)	120	175	130
Fracture spatial distribution			
Distribution	power law	power law	power law
n	0.53	0.73	0.78
Minimum distance (m)	1	7.5	7.5
Maximum distance (m)	600	600	600
Buffer zone			
Method	constant	constant	constant
Size (m)	1.4	0.8	1.7

Figure 6 compares the data for fracture length, spacing and orientation observed at the Apodi outcrop with the best-fitting distribution functions (Table 2). Throughout this example, we take the raw data for the Apodi outcrop as the truth. In all scenarios, the statistical properties for the generated fracture networks are consistent with the best-fitting distribution functions. While this is to be expected, we discussed above that situations are possible where fracture saturation is reached before all fractures can be placed in the network and input and output statistics for the fracture network are inconsistent. This is not the case here because the raw data are geologically consistent. Note that when fitting distribution functions to the fracture spacing using SciPy (Fig. 6), we tested all PDFs listed in Table 1. Among these, the power-law distribution provided the best statistical fit, although it may appear that a log-normal distribution may also yield a good fit.

Figures 7–9 show ten equiprobable statistical realizations of the fracture network for Scenarios A, B and C, respectively. For Scenario A, the locations of the fracture clusters for each fracture set vary noticeably from the locations observed in the outcrop data. This situation is improved in Scenario B because the first fracture of each set is placed in the region where the clusters are observed in the outcrop. Hence, the spatial arrangement of the fractures appears visually more consistent with outcrop observations. In Scenario C where fractures are not placed in areas where the outcrop is covered by vegetation, the consistency between modelled and observed fracture distributions improves further. We note that these comparisons are only qualitative. A more quantitative comparison that evaluates the impact of the different fracture network geometries on heat flow will be discussed below.

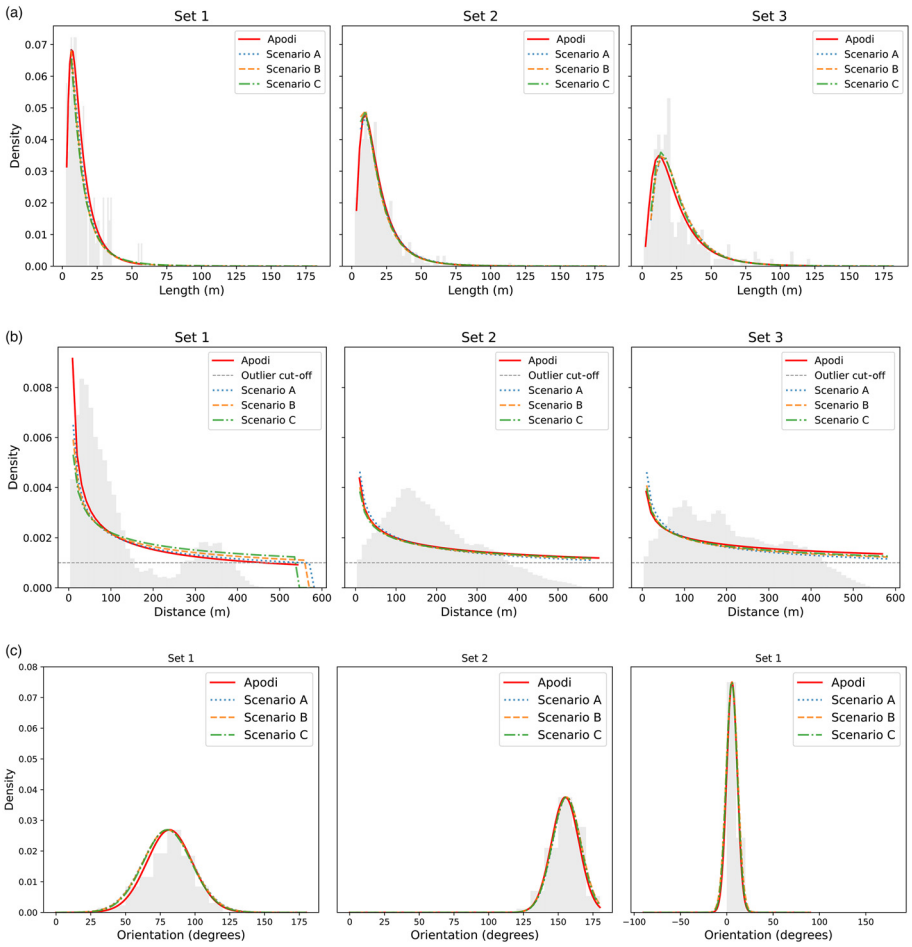

Fig. 6. Comparison of the raw data (grey bins) observed for (**a**) fracture length, (**b**) fracture spacing and (**c**) fracture orientation at the Apodi outcrop with the best-fitting distribution functions from Table 1 and the statistics obtained for the generated fracture networks.

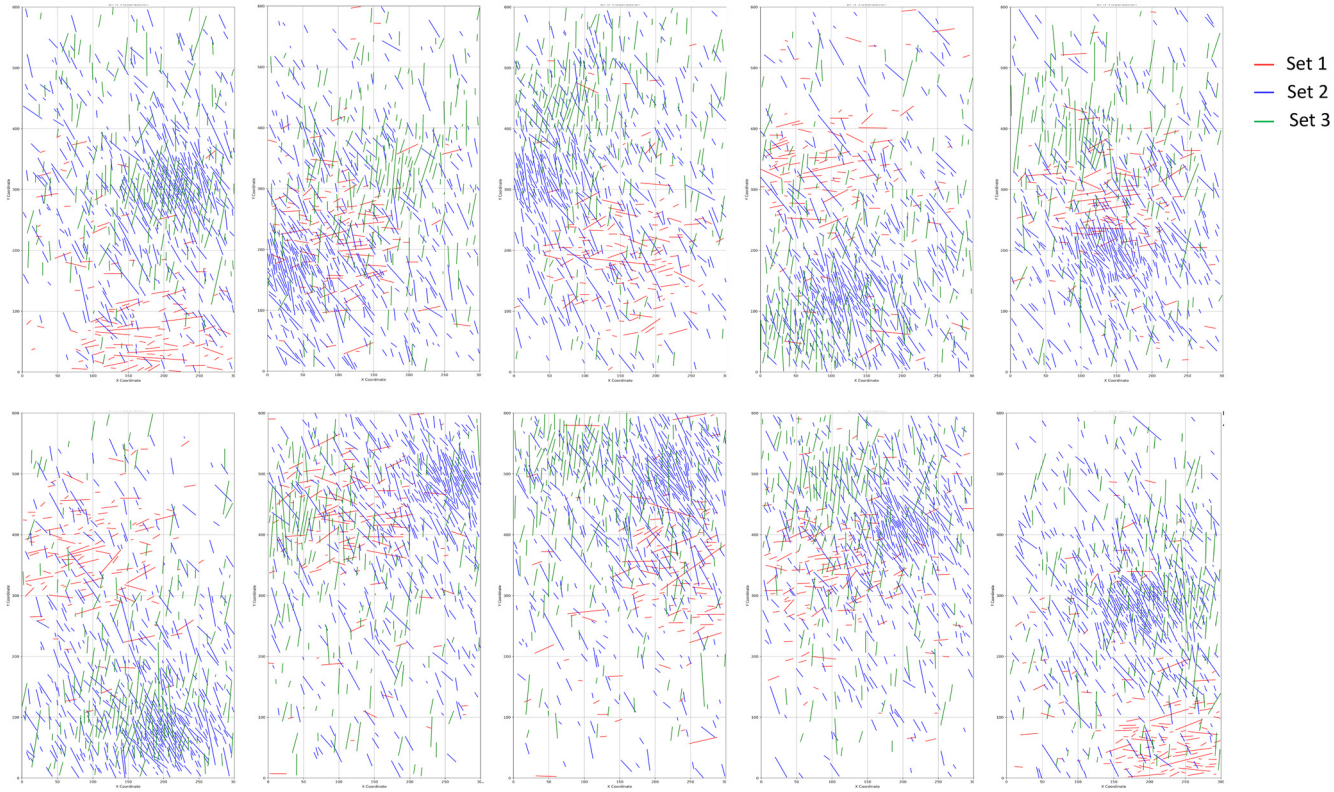

Fig. 7. Ten equally probable realizations of the fracture networks generated for Scenario A.

However, even this qualitative comparison indicates that there are differences in the configuration of the individual fractures in the generated networks and the network observed in the outcrop. The outcrop appears to contain a small number of comparatively long fractures (Fig. 5). Upon closer inspection, these longer fractures consist of shorter, disconnected segments in the raw data. In other words, the raw data, which we take as the truth, do not contain these long continuous fractures. As a result, the generated networks also

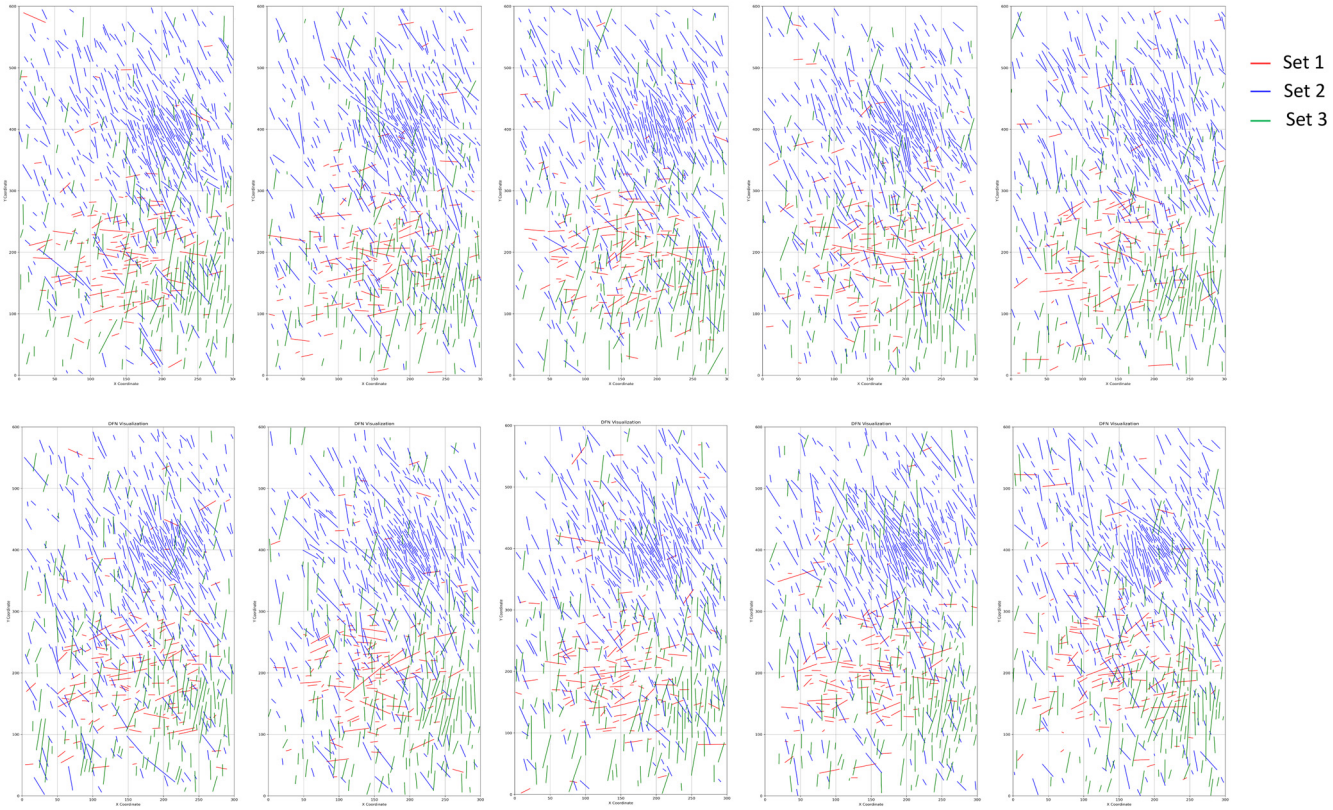

Fig. 8. Ten equally probable realizations of the fracture networks generated for Scenario B.

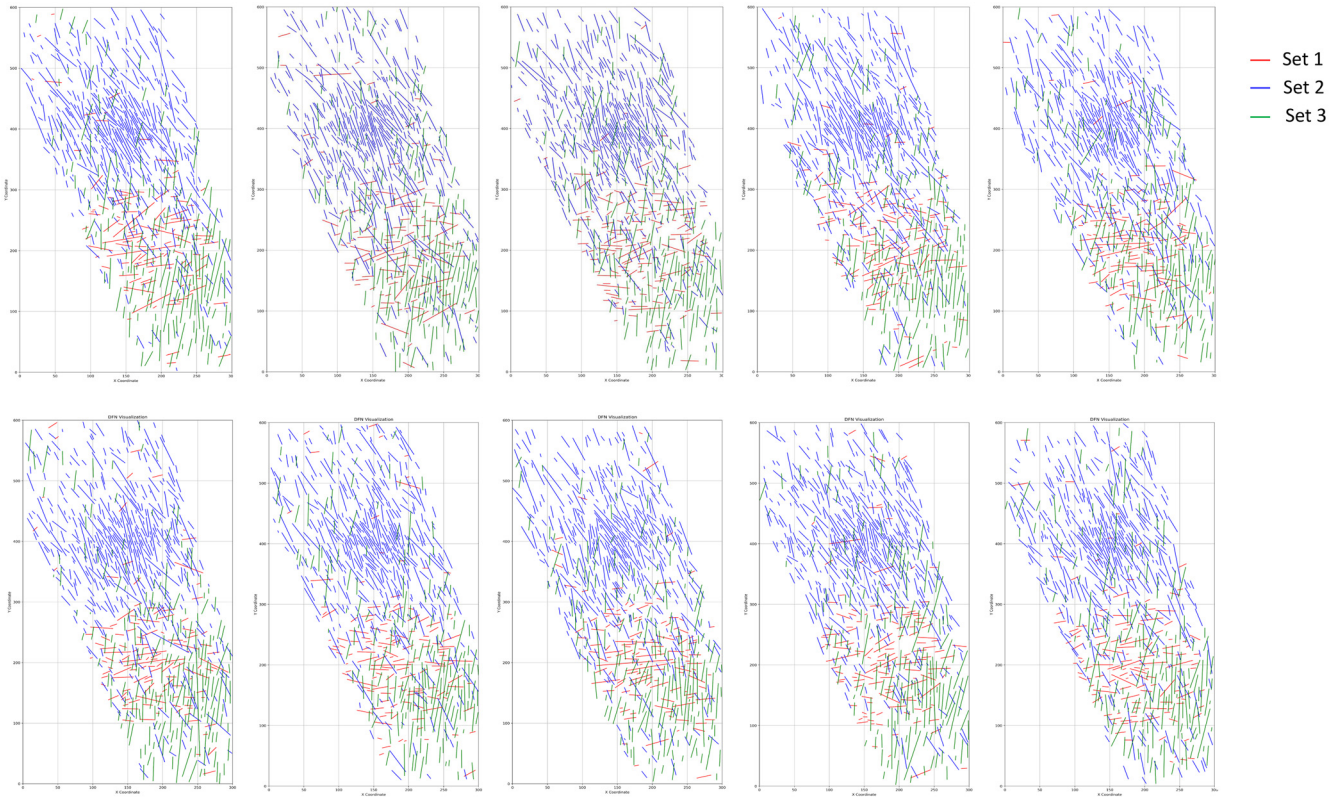

Fig. 9. Ten equally probable realizations of the fracture networks generated for Scenario C.

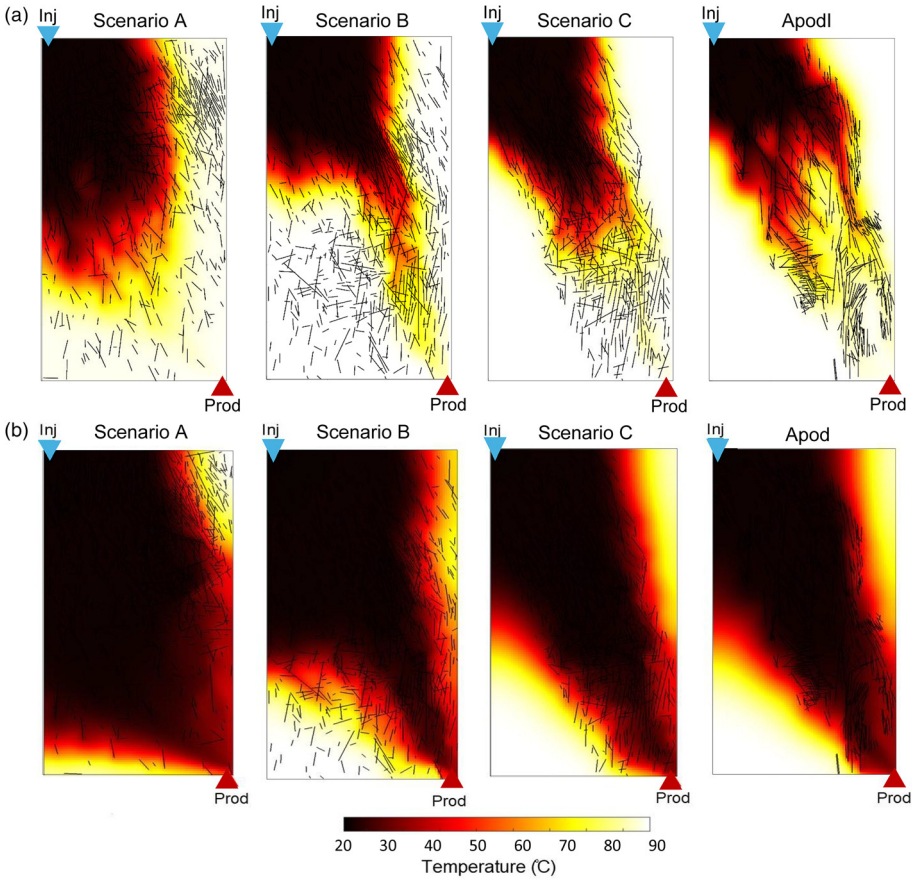

Fig. 10. Thermal front propagation at (**a**) thermal breakthrough time and (**b**) after 75 years of production for one realization from each scenario and the Apodi outcrop. Injector and producer well locations are indicated with blue downward- and red upward-pointing triangles, respectively.

lack such fractures, since they honour the length distribution derived from the raw data (Fig. 6). Without revisiting the Apodi outcrop in Brazil, it is very difficult to assess if these segments are observed in nature or if the outcrop indeed contains a few longer fractures that have been stored as smaller segments in the raw data.

Comparative analysis of thermal behaviour

We now perform geothermal heat flow simulations using MRST (Collignon *et al*. 2021) for the fracture network mapped at the Apodi outcrop and compare it to the heat flow behaviour computed for each of the ten fracture networks that were generated for Scenarios A, B and C. This allows us to compare the level of similarity between the heat flow behaviour for the stochastically generated fracture networks and the heat flow behaviour in the fracture network observed in the outcrop. We consider the Apodi outcrop and its heat flow behaviour as the reference solution.

The simulations aim to quantify how variations in the spatial organization of the fractures affect thermal front propagation and thermal breakthrough time. To this end, we simulate a geothermal doublet system comprising one injector and one producer placed at the NW and SE corners of the domain, respectively. We use a pseudo-3D model assuming a constant vertical thickness of 10 m, which allows us to approximate volumetric flow while keeping computational costs manageable. The reservoir temperature is set to 90°C. To isolate the effects of fracture geometry on thermal behaviour, we assume a uniform fracture aperture of 0.001 m and apply similar reservoir and fluid properties, boundary conditions and operational settings across all scenarios. The matrix permeability was set to 10^{-15} m^2 to emphasize the influence of fractures (Lei *et al*. 2015). We choose an injection rate of 50 m^3/day at 25°C, which reflects a moderate production rate for this domain where both advective and conductive heat transport contribute to the thermal response.

We first conduct a qualitative comparison of the temperature distribution at thermal breakthrough time and after 75 years of production for one realization from each scenario with the 'truth case' from the Apodi outcrop (Fig. 10). For the purpose of this comparison, we assume that the fractures mapped from drone imagery fully represent the network, and that no fractures are present in areas covered by vegetation. At thermal breakthrough (Fig. 10a), the Apodi outcrop exhibits a heterogeneous thermal front with well-developed preferential flow paths, which align with the clustered and anisotropic structure of the mapped fracture network. In contrast, Scenario A, which assumes randomly distributed fractures across the entire model geometry, shows a uniform thermal front without localized heat flow. Scenarios B and C show progressively better alignment with the Apodi outcrop, exhibiting increased flow channelling and anisotropic thermal front propagation. This alignment arises from improved geological consistency with the outcrop, achieved by incorporating fracture sets in the regions where clustering is observed in the outcrop (Scenario B) and also excluding areas covered by vegetation (Scenario C). After 75 years of production (Fig. 10b), the differences in long-term thermal front propagation and thermal recovery become evident. The Apodi outcrop exhibits a channelized thermal front with clear anisotropy, and parts of the reservoir remain largely unaffected by thermal front propagation. Scenarios B and C also show directional thermal front propagation and closely resemble the thermal front behaviour observed in the Apodi outcrop, including focused heat extraction and the presence of unswept regions away from dominant flow paths. In contrast, Scenario A displays a uniform thermal front and nearly complete thermal sweep, which does not capture the spatial heterogeneity observed in the outcrop and leads to an optimistic prediction of reservoir performance.

We then evaluate thermal breakthrough behaviour using Lifetime Production (LTP) metrics, which quantify the time required for

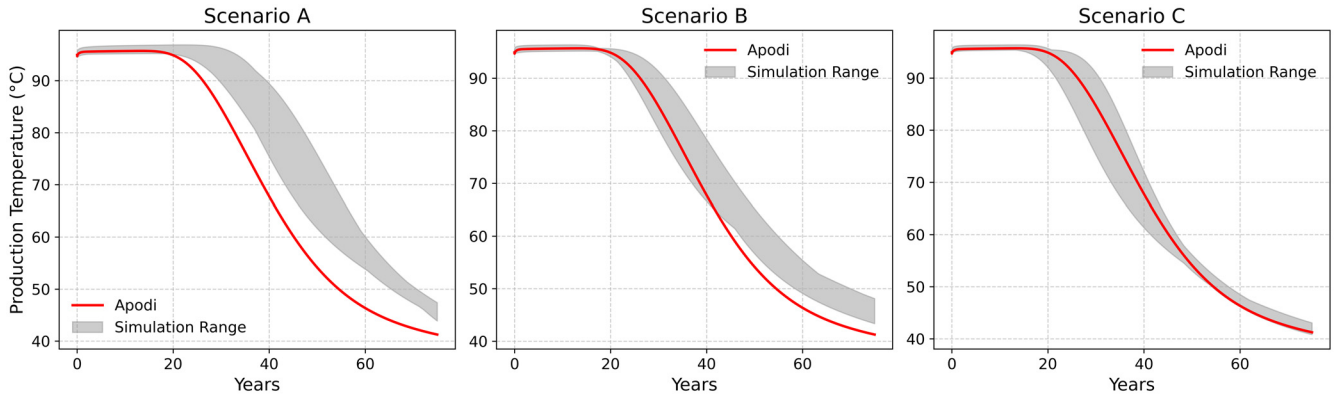

Fig. 11. Comparison of production temperature decline over time for the Apodi outcrop (red) and the simulation ranges defined by the minimum and maximum values across ten stochastic realizations for each fracture network scenario (grey).

production temperature to decline by 1°C (LTP), 5°C (LTP_5) and 10°C (LTP_{10}) relative to the initial reservoir temperature (Fig. 11; Table 3). These thresholds serve as standardized indicators of thermal performance and economic viability in geothermal systems (Babaei and Nick 2019). Scenario A significantly overpredicts system performance, with a delayed breakthrough time compared to the Apodi outcrop. This discrepancy in LTP arises from the absence of fracture clustering and anisotropy, which reduces preferential flow and leads to unrealistically uniform cooling. Scenarios B and C progressively improve agreement with the reference case. Scenario B demonstrates faster breakthrough due to partial fracture alignment, while Scenario C nearly replicates the Apodi outcrop's behaviour for all LTP thresholds.

These findings underscore that even with multiple stochastic realizations, the thermal behaviour observed in outcrop data cannot be reliably reproduced unless the fracture patterns are represented in a geologically consistent manner. This highlights the importance of using an integrated workflow that combines geologically constrained fracture network generation with dynamic simulations, such as the one developed in this study, to enable more reliable predictions of subsurface heat flow.

Transition from matrix-dominated to fracture-dominated fluid flow

We now illustrate the proposed workflow by applying it to the classic problem of identifying when fluid flow in fractured geological formations transitions from matrix-dominated to fracture-dominated. We therefore generate an ensemble of fracture networks. Specifically, we generate five equiprobable fracture networks for a range of increasing areal fracture intensities P_{21}, which vary from 0.005 to 0.5 m^{-1} (Table 4). We then calculate the effective fracture–matrix permeability to investigate when fluid flow starts to be dominated by the fracture network because the fractures start to connect, meaning that the network reaches the percolation threshold.

Figure 12 shows the evolution of the effective fracture–matrix permeability, along with example fracture network geometries for selected P_{21} values. Initially, owing to the low fracture intensity and poor connectivity of the fractures, the effective permeability is only slightly higher than that of the rock matrix, so the fracture and matrix act as a single-porosity system (Wong *et al.* 2020). As the fractures become connected, the effective fracture–matrix permeability increases rapidly, indicating that the fractures start to dominate flow. The variation in effective permeability between individual realizations is largest when the fractures start to provide fully connected pathways around the percolation threshold (Bogdanov *et al.* 2003; Agbaje *et al.* 2023). Unlike the previous example, which was constrained by outcrop data, generating synthetic fracture networks carries the risk of combining input parameters that are not geologically consistent or represent an over-saturated network. In this particular example, with the chosen parameter combination, the network becomes saturated as P_{21} approaches 1 m^{-1}, and the algorithm prevents adding additional fractures beyond this point. As

Table 3. Comparison of breakthrough times (LTP, LTP_5 and LTP_{10}) for the Apodi outcrop and the average across all realizations for each scenario

Scenario	LTP (yr)	LTP_5 (yr)	LTP_{10} (yr)
Apodi outcrop	22	26	30
Scenario A	30	35.5	39
Scenario B	23	28	32
Scenario C	22	26	29.5

Table 4. Input parameters used for generating fracture networks that investigate the transition from matrix-dominated to fracture-dominated flow (domain size of 200 × 200 m^2)

Parameter	Set 1	Set 2
Fracture intensity		
P_{21} (m^{-1})	0.005–0.5	0.005–0.5
Fracture length		
Distribution	log-normal	log-normal
μ (m)	2.73	2.73
σ	0.68	0.68
Minimum length (m)	2.23	2.23
Maximum length (m)	200	200
Fracture orientation		
Distribution	von Mises	von Mises
κ	24.5	24.5
μ (m)	0	1.57
Minimum orientation (degree)	−10	75
Maximum orientation (degree)	10	105
Fracture spatial distribution		
Distribution	uniform	uniform
Minimum distance (m)	1	1
Maximum distance (m)	200	200
Buffer zone		
Method	constant	constant
Size (m)	0.3	0.3
Fracture aperture		
Method	constant	constant
Size (m)	0.001	0.001

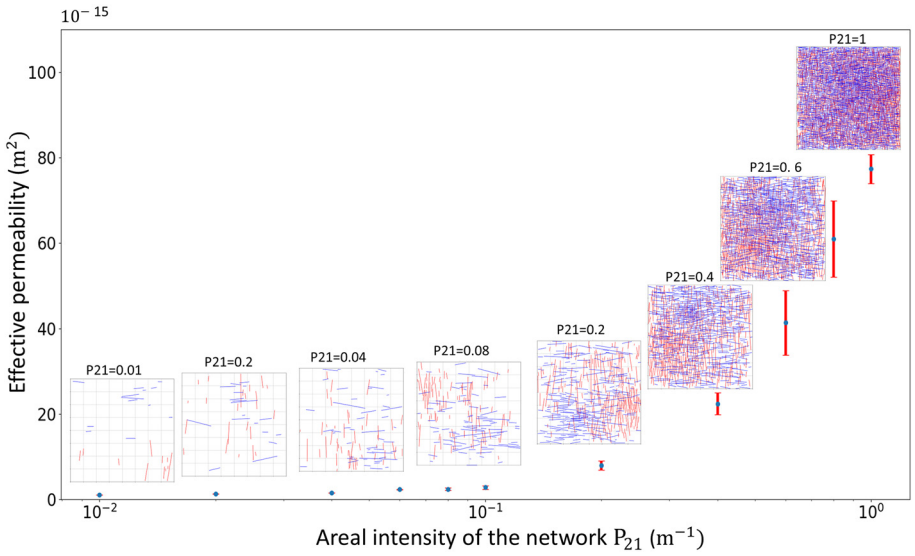

Fig. 12. Evolution of the effective fracture–matrix permeability for different fracture networks as a function of the areal fracture intensity P_{21}. The insets show example networks at selected fracture intensities.

a result, networks with P_{21} values higher than this threshold cannot be generated, so their effective permeability cannot be computed. Hence, a plateau in effective fracture–matrix permeability for P_{21} values much larger than 1 m^{-1} is not observed, although it has been documented in other studies (Agbaje *et al.* 2023). While it is possible to reach higher P_{21} values by adjusting other parameters, for example reducing the stress shadow size, this was not done in this study as our aim was to solely observe the effect of P_{21} on effective permeability by keeping all other parameters constant.

Conclusions

This study presents an integrated workflow, made available as open-source code written in Python, that generates geologically plausible fracture networks from fracture attributes derived from various surface and subsurface sources and utilizes these networks in flow and transport simulations. Although outcrop-based flow and transport modelling studies have yielded important insights into the fundamental aspects of fluid and heat flow in fractured geological formations, such studies are largely deterministic and do not allow for a more comprehensive uncertainty analysis that robustly quantifies how different properties of a fracture network affect flow and heat transfer processes.

The proposed workflow is based on a computationally efficient hybrid approach that combines mechanical and statistical methods to generate geologically plausible fracture networks. It is therefore possible to quickly create a large ensemble of fracture networks that explores uncertainties related to fracture intensity, fracture orientation, fracture aperture distribution and fracture connectivity. The resulting ensemble can be deployed in multi-purpose simulators, such as MRST that allows for an explicit representation of the fracture network, to perform simulations of fluid and heat transfer in fractured porous media. Such an integrated approach addresses a recently identified knowledge gap: the workflow paves the way for generating the input data needed to develop machine-learning based emulators that quantify uncertainties related to flow and transport in complex fracture networks relevant to subsurface applications such as groundwater contamination, geothermal energy production or CO_2 storage.

This workflow is illustrated using two well-known example applications. First, fracture networks are generated stochastically and compared qualitatively to a fracture network observed in an outcrop analogue. Heat flow simulations are then performed on all fracture networks to quantitatively compare the thermal evolution and heat production between the stochastic networks and the network observed in the outcrop. Second, an ensemble of fracture networks is generated with increasingly larger fracture intensities to analyse when fluid flow changes from matrix-dominated to fracture-dominated. These applications demonstrate the ease with which geologically plausible fracture networks can be generated and utilized in subsequent fluid flow simulations.

Acknowledgements The authors thank Energi Simulation for funding this research. We also thank Micheal Welch and one anonymous reviewer for their constructive feedback and insightful comments that helped us to improve the original manuscript. We also acknowledge Jasper Hupkes for insightful discussions on fracture networks.

Author contributions **EK**: conceptualization (lead), data curation (lead), formal analysis (lead), investigation (lead), methodology (lead), software (lead), validation (lead), visualization (lead), writing – original draft (lead), writing – review & editing (lead); **P-OB**: data curation (equal), formal analysis (equal), funding acquisition (equal), investigation (equal), methodology (equal), project administration (equal), resources (equal), software (equal), supervision (equal), validation (equal), visualization (equal), writing – original draft (equal), writing – review & editing (equal); **AD**: conceptualization (equal), data curation (equal), formal analysis (equal), funding acquisition (equal), investigation (equal), methodology (equal), project administration (equal), resources (equal), software (equal), supervision (equal), validation (equal), visualization (equal), writing – original draft (equal), writing – review & editing (equal); **GR**: conceptualization (equal), data curation (equal), formal analysis (equal), funding acquisition (equal), investigation (equal), methodology (equal), project administration (equal), resources (equal), software (equal), supervision (equal), validation (equal), visualization (equal), writing – original draft (equal), writing – review & editing (equal); **SG**: conceptualization (lead), data curation (equal), formal analysis (lead), funding acquisition (lead), investigation (lead), methodology (lead), project administration (lead), resources (lead), software (equal), supervision (lead), validation (lead), visualization (lead), writing – original draft (lead), writing – review & editing (lead)

Funding This work was funded by the Energi Simulation.

Competing interests The authors declare that they have no known competing financial interests or personal relationships that could have appeared to influence the work reported in this paper.

Data availability The datasets generated during and/or analysed during the current study are available in the 4TU. ResearchData repository, https://data.4tu.nl/datasets/0dc9c47a-2294-4811-a0fe-e049cb15ff3d. The open-source GeoDFN software can be downloaded from 4TU. ResearchData using https://doi.org/10.4121/0dc9c47a-2294-4811-a0fe-e049cb15ff3d.v1. This repository also includes the code to link GeoDFN output to SINTEF's open-source Matlab Reservoir Simulation Toolbox (MRST) for subsequent fluid flow modelling. MRST can be downloaded from https://www.sintef.no/projectweb/mrst/. The raw data for the Apodi outcrop can be accessed using https://doi.org/10.4121/uuid:988152da-3ac3-44cb-9d87-c7365e3707b6.

Appendix A. Additional input data

The input parameters to generate the fracture networks shown in Figure 2 are given in Tables A1 and A2.

Table A1. Input parameters used for generating the example fracture networks in Figure 2 (domain size of 1000 × 1000 m^2)

Parameter	Set 1	Set 2
Fracture intensity		
P_{21}* (m^{-1})	0.03	0.03
Fracture length		
Distribution	power-law	power-law
n	2.5	2.5
Minimum length (m)	5	5
Maximum length (m)	100	1000
Fracture orientation		
Distribution	von Mises	von Mises
κ	300	300
μ (radian)	0	1.047
Fracture spatial distribution		
Distribution	log-normal	log-normal
μ (m)	5.521	5.521
σ	0.7	0.7
Maximum distance (m)	1000	1000
Stress shadow		
Method*	constant	constant
Size* (m)	4	4

Parameters denoted with a star are modified to generate the examples.

Table A2. Parameters and values used for calculating fracture apertures in Figure 2 using the Barton–Bandis method (Barton et al. 1985)

Parameter	Value
JCS (MPa)	140
JRC	15
$\sigma_{H_{max}}$ (MPa)	140
σ_c (MPa)	140
Azimuth (degrees)	[0°, 45°, 90°]

JCS, Joint Wall Compressive Strength; JRC, Joint Roughness Coefficient.

References

Agbaje, T.Q., Ghanbarian, B. and Hyman, J.D. 2023. Effective permeability in fractured reservoirs: discrete fracture matrix simulations and percolation-based effective-medium approximation. *Water Resources Research*, **59**, e2023WR036505, https://doi.org/10.1029/2023WR036505

Alain, T. and Vincent, R. 2004. Hydro-mechanical upscaling of a fractured rockmass using a 3D numerical approach. *Elsevier Geo-Engineering Book Series*, **2**, 275–280, https://doi.org/10.1016/S1571-9960(04)80053-3

Andre, B.J. and Rajaram, H. 2005. Dissolution of limestone fractures by cooling waters: early development of hypogene karst systems. *Water Resources Research*, **41**, 1–16, https://doi.org/10.1029/2004WR003331

Andrianov, N. and Nick, H.M. 2021. Machine learning of dual porosity model closures from discrete fracture simulations. *Advances in Water Resources*, **147**, 103810, https://doi.org/10.1016/J.ADVWATRES.2020.103810

Ashworth, M., Elsheikh, A.H. and Doster, F. 2022. Machine learning-based multiscale constitutive modelling: development and application to dual-porosity mass transfer. *Advances in Water Resources*, **163**, 104166, https://doi.org/10.1016/J.ADVWATRES.2022.104166

Atkinson, B.K. 1982. Subcritical crack propagation in rocks: theory, experimental results and applications. *Journal of Structural Geology*, **4**, 41–56, https://doi.org/10.1016/0191-8141(82)90005-0

Atkinson, C. and Craster, R.V. 1995. Theoretical aspects of fracture mechanics. *Progress in Aerospace Sciences*, **31**, 1–83, https://doi.org/10.1016/0376-0421(93)E0001-M

Babaei, M. and Nick, H.M. 2019. Performance of low-enthalpy geothermal systems: interplay of spatially correlated heterogeneity and well-doublet spacings. *Applied Energy*, **253**, 113569, https://doi.org/10.1016/J.APENERGY.2019.113569

Bai, T. and Pollard, D.D. 2000*a*. Closely spaced fractures in layered rocks: initiation mechanism and propagation kinematics. *Journal of Structural Geology*, **22**, 1409–1425, https://doi.org/10.1016/S0191-8141(00)00062-6

Bai, T. and Pollard, D.D. 2000*b*. Fracture spacing in layered rocks: a new explanation based on the stress transition. *Journal of Structural Geology*, **22**, 43–57, https://doi.org/10.1016/S0191-8141(99)00137-6

Bai, T., Pollard, D.D. and Gao, H. 2000. Explanation for fracture spacing in layered materials. *Nature*, **403**, 753–756, https://doi.org/10.1038/35001550

Bai, T., Maerten, L., Gross, M.R. and Aydin, A. 2002. Orthogonal cross joints: do they imply a regional stress rotation? *Journal of Structural Geology*, **24**, 77–88, https://doi.org/10.1016/S0191-8141(01)00050-5

Barton, N., Bandis, S. and Bakhtar, K. 1985. Strength, deformation and conductivity coupling of rock joints. *International Journal of Rock Mechanics and Mining Sciences & Geomechanics Abstracts*, **22**, 121–140, https://doi.org/10.1016/0148-9062(85)93227-9

Bellian, J.A., Kerans, C. and Jennette, D.C. 2005. Digital outcrop models: applications of terrestrial scanning lidar technology in stratigraphic modeling. *Journal of Sedimentary Research*, **75**, 166–176, https://doi.org/10.2110/JSR.2005.013

Berkowitz, B. 2002. Characterizing flow and transport in fractured geological media: a review. *Advances in Water Resources*, **25**, 861–884, https://doi.org/10.1016/S0309-1708(02)00042-8

Berre, I., Doster, F. and Keilegavlen, E. 2019. Flow in fractured porous media: a review of conceptual models and discretization approaches. *Transport in Porous Media*, **130**, 215–236, https://doi.org/10.1007/s11242-018-1171-6

Berrone, S., Canuto, C., Pieraccini, S. and Scialò, S. 2018. Uncertainty quantification in discrete fracture network models: stochastic geometry. *Water Resources Research*, **54**, 1338–1352, https://doi.org/10.1002/2017WR021163

Bisdom, K., Bertotti, G. and Nick, H.M. 2016*a*. The impact of in-situ stress and outcrop-based fracture geometry on hydraulic aperture and upscaled permeability in fractured reservoirs. *Tectonophysics*, **690**, 63–75, https://doi.org/10.1016/j.tecto.2016.04.006

Bisdom, K., Bertotti, G. and Nick, H.M. 2016*b*. The impact of different aperture distribution models and critical stress criteria on equivalent permeability in fractured rocks. *Journal of Geophysical Research: Solid Earth*, **121**, 4045–4063, https://doi.org/10.1002/2015JB012657

Bisdom, K., Bertotti, G. and Bezerra, F.H. 2017*a*. Inter-well scale natural fracture geometry and permeability variations in low-deformation carbonate rocks. *Journal of Structural Geology*, **97**, 23–36, https://doi.org/10.1016/J.JSG.2017.02.011

Bisdom, K., Nick, H.M. and Bertotti, G. 2017*b*. An integrated workflow for stress and flow modelling using outcrop-derived discrete fracture networks. *Computers & Geosciences*, **103**, 21–35, https://doi.org/10.1016/J.CAGEO.2017.02.019

Boersma, Q.D. 2020. *Natural Fracture Network Characterisation: Numerical Modelling, Outcrop Analysis and Subsurface Data*. PhD thesis, Delft University of Technology.

Bogdanov, I.I., Mourzenko, V.V., Thovert, J.-F. and Adler, P.M. 2003. Effective permeability of fractured porous media with power-law distribution of fracture sizes. *Physical Review E*, **76**, 036309, https://doi.org/10.1103/PhysRevE.76.036309

Bonneau, F., Henrion, V., Caumon, G., Renard, P. and Sausse, J. 2013. A methodology for pseudo-genetic stochastic modeling of discrete fracture networks. *Computers & Geosciences*, **56**, 12–22, https://doi.org/10.1016/J.CAGEO.2013.02.004

Bonnet, E., Bour, O., Odling, N.E., Davy, P., Main, I., Cowie, P. and Berkowitz, B. 2001. Scaling of fracture systems in geological media. *Reviews of Geophysics*, **39**, 347–383, https://doi.org/10.1029/1999RG000074

Collignon, M., Klemetsdal, Ø.S. and Møyner, O. 2021. Simulation of geothermal systems using MRST. *In:* Lie, K.-A. and Møyner, O. (eds) *Advanced Modeling with the MATLAB Reservoir Simulation Toolbox*. Cambridge University Press, 491–514, https://doi.org/10.1017/9781009019781.018

Darcel, C., Davy, P., Le Goc, R., de Dreuzy, J.R. and Bour, O. 2009. *Statistical Methodology for Discrete Fracture Model – Including Fracture Size, Orientation Uncertainty Together with Intensity Uncertainty and Variability*. Technical report **R-09-38**. Svensk Kärnbränslehantering AB.

Davy, P., Le Goc, R. and Darcel, C. 2013. A model of fracture nucleation, growth and arrest, and consequences for fracture density and scaling. *Journal of Geophysical Research: Solid Earth*, **118**, 1393–1407, https://doi.org/10.1002/JGRB.50120

Davy, P., Le Goc, R. and Darcel, C. 2014. A non-Poissonian, likely-universal, fracture model for hardrock DFN. Proceedings of the First International Conference on Discrete Fracture Network Engineering, 19–22 October 2014, Vancouver, Canada.

de Dreuzy, J.R., Davy, P. and Bour, O. 2001. Hydraulic properties of two-dimensional random fracture networks following a power law length distribution: 1. Effective connectivity. *Water Resources Research*, **37**, 2065–2078, https://doi.org/10.1029/2001WR900011

de Dreuzy, J.R., Darcel, C., Davy, P. and Bour, O. 2004. Influence of spatial correlation of fracture centers on the permeability of two-dimensional fracture networks following a power law length distribution. *Water Resources Research*, **40**, W01502, https://doi.org/10.1029/2003WR002260

de Hoop, S., Voskov, D.V., Bertotti, G. and Barnhoorn, A. 2022. An advanced discrete fracture methodology for fast, robust, and accurate simulation of

energy production from complex fracture networks. *Water Resources Research*, **58**, e2021WR030743, https://doi.org/10.1029/2021WR030743

Denetto, S. and Kamp, A.M. 2016. Cubic law evaluation using well test analysis for fractured reservoir characterization. Paper SPE-181410-MS, presented at the SPE Annual Technical Conference and Exhibition, 26–28 September 2016, Dubai, UAE, https://doi.org/10.2118/181410-MS

Dershowitz, W.S. 1984. *Rock Joint Systems*. PhD thesis, Massachusetts Institute of Technology.

Dershowitz, W.S. and Herda, H.H. 1992. Interpretation of fracture spacing and intensity. Paper ARMA-92-0757, presented at The 33rd U.S. Symposium on Rock Mechanics (USRMS), 3–5 June 1992, Santa Fe, New Mexico.

Edery, Y., Geiger, S. and Berkowitz, B. 2016. Structural controls on anomalous transport in fractured porous rock. *Water Resources Research*, **52**, 5634–5643, https://doi.org/10.1002/2016WR018942

Fadakar Alghalandis, Y., Xu, C. and Dowd, P.A. 2011. A general framework for fracture intersection analysis: algorithms and practical applications. *In:* Budd, A.R. (ed.) Proceedings of the 2011 Australian Geothermal Energy Conference, 16–18 November 2011, Melbourne, Australia, 15–20.

Flemisch, B., Darcis, M. *et al.* 2011. DuMux: DUNE for multi-{phase, component, scale, physics, …} flow and transport in porous media. *Advances in Water Resources*, **34**, 1102–1112, https://doi.org/10.1016/J.ADVWATRES.2011.03.007

Flemisch, B., Fumagalli, A. and Scotti, A. 2016. A review of the XFEM-based approximation of flow in fractured porous media. *In*: Ventura, G. and Benvenuti, E. (eds) *Advances in Discretization Methods*. SEMA SIMAI Springer Series, **12**, 47–76, https://doi.org/10.1007/978-3-319-41246-7_3

Flemisch, B., Berre, I. *et al.* 2018. Benchmarks for single-phase flow in fractured porous media. *Advances in Water Resources*, **111**, 239–258, https://doi.org/10.1016/J.ADVWATRES.2017.10.036

Freites, A., Corbett, P., Rongier, G. and Geiger, S. 2023. Automated classification of well test responses in naturally fractured reservoirs using unsupervised machine learning. *Transport in Porous Media*, **147**, 747–779, https://doi.org/10.1007/S11242-023-01929-1

Fumagalli, A., Pasquale, L., Zonca, S. and Micheletti, S. 2016. An upscaling procedure for fractured reservoirs with embedded grids. *Water Resources Research*, **52**, 6506–6525, https://doi.org/10.1002/2015WR017729

Geiger, S. and Emmanuel, S. 2010. Non-Fourier thermal transport in fractured geological media. *Water Resources Research*, **46**, W07504, https://doi.org/10.1029/2009WR008671

Geiger, S. and Matthäi, S. 2014. What can we learn from high-resolution numerical simulations of single- and multi-phase fluid flow in fractured outcrop analogues? *Geological Society, London, Special Publications*, **374**, 125–144, https://doi.org/10.1144/SP374.8

Geiger, S., Cortis, A. and Birkholzer, J.T. 2010. Upscaling solute transport in naturally fractured porous media with the continuous time random walk method. *Water Resources Research*, **46**, 12530, https://doi.org/10.1029/2010WR009133

Gierzynski, A.O. and Pollyea, R.M. 2017. Three-phase CO_2 flow in a basalt fracture network. *Water Resources Research*, **53**, 8980–8998, https://doi.org/10.1002/2017WR021126

Gillespie, P.A., Howard, C.B., Walsh, J.J. and Watterson, J. 1993. Measurement and characterisation of spatial distributions of fractures. *Tectonophysics*, **226**, 113–141, https://doi.org/10.1016/0040-1951(93)90114-Y

Griffith, A.A. 1921. VI. The phenomena of rupture and flow in solids. *Philosophical Transactions of the Royal Society of London. Series A, Containing Papers of a Mathematical or Physical Character*, **4**, 9–14, https://doi.org/10.1098/RSTA.1921.0006

Gutierrez, M. and Youn, D.J. 2015. Effects of fracture distribution and length scale on the equivalent continuum elastic compliance of fractured rock masses. *Journal of Rock Mechanics and Geotechnical Engineering*, **7**, 626–637, https://doi.org/10.1016/J.JRMGE.2015.07.006

Hardebol, N.J., Maier, C., Nick, H., Geiger, S., Bertotti, G. and Boro, H. 2015. Multiscale fracture network characterization and impact on flow: a case study on the Latemar carbonate platform. *Journal of Geophysical Research: Solid Earth*, **120**, 8197–8222, https://doi.org/10.1002/2015JB011879

He, C., Yao, C., Jin, Y., Jiang, Q. and Zhou, C. 2023. Effective permeability of fractured porous media with fracture density near the percolation threshold. *Applied Mathematical Modelling*, **117**, 592–608, https://doi.org/10.1016/J.APM.2023.01.010

Healy, D., Rizzo, R.E. *et al.* 2017. FracPaQ: a MATLAB™ toolbox for the quantification of fracture patterns. *Journal of Structural Geology*, **95**, 1–16, https://doi.org/10.1016/J.JSG.2016.12.003

Hooker, J.N., Laubach, S.E. and Marrett, R. 2013. Fracture-aperture size – frequency, spatial distribution, and growth processes in strata-bounded and non-strata-bounded fractures, Cambrian Mesón Group, NW Argentina. *Journal of Structural Geology*, **54**, 54–71, https://doi.org/10.1016/J.JSG.2013.06.011

Hooker, J.N., Laubach, S.E. and Marrett, R. 2014. A universal power-law scaling exponent for fracture apertures in sandstones. *GSA Bulletin*, **126**, 1340–1362, https://doi.org/10.1130/B30945.1

Hope, S.M., Davy, P., Maillot, J., Le Goc, R. and Hansen, A. 2015. Topological impact of constrained fracture growth. *Frontiers in Physics*, **3**, 160786, https://doi.org/10.3389/FPHY.2015.00075

Huang, L., Su, X. and Tang, H. 2020. Optimal selection of estimator for obtaining an accurate three-dimensional rock fracture orientation distribution. *Engineering Geology*, **270**, 105575, https://doi.org/10.1016/J.ENGGEO.2020.105575

Iñigo, J.F., Laubach, S.E. and Hooker, J.N. 2012. Fracture abundance and patterns in the Subandean fold and thrust belt, Devonian Huamampampa Formation petroleum reservoirs and outcrops, Argentina and Bolivia. *Marine and Petroleum Geology*, **35**, 201–218, https://doi.org/10.1016/J.MARPETGEO.2012.01.010

Kang, P.K., Lei, Q., Dentz, M. and Juanes, R. 2019. Stress-induced anomalous transport in natural fracture networks. *Water Resources Research*, **55**, 4163–4185, https://doi.org/10.1029/2019WR024944

Karimi-Fard, M., Gong, B. and Durlofsky, L.J. 2006. Generation of coarse-scale continuum flow models from detailed fracture characterizations. *Water Resources Research*, **42**, 10423, https://doi.org/10.1029/2006WR005015

Keilegavlen, E., Berge, R., Fumagalli, A., Starnoni, M., Stefansson, I., Varela, J. and Berre, I. 2021. PorePy: an open-source software for simulation of multiphysics processes in fractured porous media. *Computational Geosciences*, **25**, 243–265, https://doi.org/10.1007/S10596-020-10002-5

Laubach, S.E. and Ward, M.E. 2006. Diagenesis in porosity evolution of opening-mode fractures, Middle Triassic to Lower Jurassic La Boca Formation, NE Mexico. *Tectonophysics*, **419**, 75–97, https://doi.org/10.1016/J.TECTO.2006.03.020

Lavoine, E., Davy, P., Darcel, C., Mas Ivars, D. and Kasani, H.A. 2023. Assessing stress variability in fractured rock masses with frictional properties and power law fracture size distributions. *Rock Mechanics and Rock Engineering*, **1**, 1–14, https://doi.org/10.1007/S00603-023-03683-8

Lee, S.H., Lough, M.F. and Jensen, C.L. 2001. Hierarchical modeling of flow in naturally fractured formations with multiple length scales. *Water Resources Research*, **37**, 443–455, https://doi.org/10.1029/2000WR900340

Lei, Q., Latham, J.P., Tsang, C.F., Xiang, J. and Lang, P. 2015. A new approach to upscaling fracture network models while preserving geostatistical and geomechanical characteristics. *Journal of Geophysical Research: Solid Earth*, **120**, 4784–4807, https://doi.org/10.1002/2014JB011736

Lei, Q., Latham, J.P. and Tsang, C.F. 2017. The use of discrete fracture networks for modelling coupled geomechanical and hydrological behaviour of fractured rocks. *Computers and Geotechnics*, **85**, 151–176, https://doi.org/10.1016/J.COMPGEO.2016.12.024

Lepillier, B., Daniilidis, A., Gholizadeh, N.D., Bruna, P.O., Kummerow, J. and Bruhn, D. 2019. A fracture flow permeability and stress dependency simulation applied to multi-reservoirs, multi-production scenarios analysis. *Geothermal Energy*, **7**, 1–16, https://doi.org/10.1186/S40517-019-0141-8

Lepillier, B., Bruna, P.O. *et al.* 2020. From outcrop scanlines to discrete fracture networks, an integrative workflow. *Journal of Structural Geology*, **133**, 103992, https://doi.org/10.1016/J.JSG.2020.103992

Li, L. and Lee, S.H. 2008. Efficient field-scale simulation of black oil in a naturally fractured reservoir through discrete fracture networks and homogenized media. *SPE Reservoir Evaluation & Engineering*, **11**, 750–758, https://doi.org/10.2118/103901-PA

Li, S., Kang, Z., Feng, X.T., Pan, Z., Huang, X. and Zhang, D. 2020. Three-dimensional hydrochemical model for dissolutional growth of fractures in karst aquifers. *Water Resources Research*, **56**, e2019WR025631, https://doi.org/10.1029/2019WR025631

Lie, K.-A. 2019. *An Introduction to Reservoir Simulation Using MATLAB/GNU Octave: User Guide for the MATLAB Reservoir Simulation Toolbox (MRST)*. Cambridge University Press, https://doi.org/10.1017/9781108591416

Lie, K.A., Krogstad, S., Ligaarden, I.S., Natvig, J.R., Nilsen, H.M. and Skaflestad, B. 2012. Open-source MATLAB implementation of consistent discretisations on complex grids. *Computational Geosciences*, **16**, 297–322, https://doi.org/10.1007/S10596-011-9244-4

Maillot, J., Davy, P., Le Goc, R., Darcel, C. and de Dreuzy, J.R. 2016. Connectivity, permeability, and channeling in randomly distributed and kinematically defined discrete fracture network models. *Water Resources Research*, **52**, 8526–8545, https://doi.org/10.1002/2016WR018973

March, M., Doster, F. and Geiger, S. 2018. Assessment of CO_2 storage potential in naturally fractured reservoirs with dual-porosity models. *Water Resources Research*, **54**, 1650–1668, https://doi.org/10.1002/2017WR022159

March, R., Maier, C., Doster, F. and Geiger, S. 2021. A unified framework for flow simulation in fractured reservoirs. *In:*Lie, K.-A. and Møyner, O.E. (eds) *Advanced Modeling with the MATLAB Reservoir Simulation Toolbox*. Cambridge University Press, 454–490.

Marrett, R., Ortega, O.J. and Kelsey, C.M. 1999. Extent of power-law scaling for natural fractures in rock. *Geology*, **27**, 799–802, https://doi.org/10.1130/0091-7613(1999)027<0799:EOPLSF>2.3.CO;2

Masciopinto, C., Passarella, G., Caputo, M.C., Masciale, R. and De Carlo, L. 2021. Hydrogeological models of water flow and pollutant transport in karstic and fractured reservoirs. *Water Resources Research*, **57**, e2021WR029969, https://doi.org/10.1029/2021WR029969

Masihi, M. and King, P.R. 2007. A correlated fracture network: modeling and percolation properties. *Water Resources Research*, **43**, W07439, https://doi.org/10.1029/2006WR005331

Matthai, S. 2024. How to write efficient C++ simulators using arrays of structures not structures of arrays in OpenCSMP. ECMOR 2024, **2024**, 2–5 September, Oslo, Norway, 1–21, https://doi.org/10.3997/2214-4609.202437056

Matthäi, S.K. and Belayneh, M. 2004. Fluid flow partitioning between fractures and a permeable rock matrix. *Geophysical Research Letters*, **31**, https://doi.org/10.1029/2003GL019027

Medici, G., Smeraglia, L., Torabi, A. and Botter, C. 2021. Review of modeling approaches to groundwater flow in deformed carbonate aquifers. *Groundwater*, **59**, 334–351, https://doi.org/10.1111/GWAT.13069

Min, K.B., Jing, L. and Stephansson, O. 2004. Determining the equivalent permeability tensor for fractured rock masses using a stochastic REV approach: method and application to the field data from Sellafield, UK. *Hydrogeology Journal*, **12**, 497–510, https://doi.org/10.1007/S10040-004-0331-7

Namdari, S., Baghbanan, A. and Hashemolhosseini, H. 2021. Investigation of the effect of the discontinuity direction on fluid flow in porous rock masses on a large-scale using hybrid FVM-DFN and streamline simulation. *Rudarsko-geološko-naftni zbornik*, **36**, 49–59, https://doi.org/10.17794/RGN.2021.4.5

Narr, W. and Suppe, J. 1991. Joint spacing in sedimentary rocks. *Journal of Structural Geology*, **13**, 1037–1048, https://doi.org/10.1016/0191-8141(91)90055-N

Narr, W., Schechter, D.S. and Thompson, L.B. 2006. *Naturally Fractured Reservoir Characterization*. Society of Petroleum Engineers.

Nick, H.M. and Matthäi, S.K. 2011. Comparison of three FE-FV numerical schemes for single- and two-phase flow simulation of fractured porous media. *Transport in Porous Media*, **90**, 421–444, https://doi.org/10.1007/S11242-011-9793-Y

Nur, A. 1982. The origin of tensile fracture lineaments. *Journal of Structural Geology*, **4**, 31–40, https://doi.org/10.1016/0191-8141(82)90004-9

Odling, N.E. and Roden, J.E. 1997. Contaminant transport in fractured rocks with significant matrix permeability, using natural fracture geometries. *Journal of Contaminant Hydrology*, **27**, 263–283, https://doi.org/10.1016/S0169-7722(96)00096-4

Olson, J.E. 1997. Natural fracture pattern characterization using a mechanically-based model constrained by geologic data – moving closer to a predictive tool. *International Journal of Rock Mechanics and Mining Sciences*, **34**, 171.e1–171.e12, https://doi.org/10.1016/S1365-1609(97)00041-5

Olson, J.E. 2003. Sublinear scaling of fracture aperture versus length: an exception or the rule? *Journal of Geophysical Research: Solid Earth*, **108**, https://doi.org/10.1029/2001JB000419

Olson, J.E. 2004. Predicting fracture swarms – the influence of subcritical crack growth and the crack-tip process on joint spacing in rock. *Geological Society, London, Special Publications*, **231**, 73–87, https://doi.org/10.1144/GSL.SP.2004.231.01.05

Olson, J.E. 2007. Fracture aperture, length and pattern geometry development under biaxial: a numerical study with applications to natural, cross-jointed systems. *Geological Society, London, Special Publications*, **289**, 123–142, https://doi.org/10.1144/SP289.8

Olson, J.E., Qiu, Y., Holder, J. and Rijken, P. 2001. Constraining the spatial distribution of fracture networks in naturally fractured reservoirs using fracture mechanics and core measurements. Proceedings – SPE Annual Technical Conference and Exhibition, 30 September–3 October 2001, New Orleans, USA, 279–290, https://doi.org/10.2118/71342-MS

Paluszny, A., Thomas, R.N., Saceanu, M.C. and Zimmerman, R.W. 2020. Hydro-mechanical interaction effects and channelling in three-dimensional fracture networks undergoing growth and nucleation. *Journal of Rock Mechanics and Geotechnical Engineering*, **12**, 707–719, https://doi.org/10.1016/J.JRMGE.2020.04.004

Pezzulli, E., Zulian, P., Kopaničáková, A., Krause, R. and Driesner, T. 2025. The limitations of a standard phase-field model in reproducing jointing in sedimentary rock layers. *International Journal for Numerical and Analytical Methods in Geomechanics*, **49**, 2709–2727, https://doi.org/10.1002/nag.4006

Pollard, D.D. and Aydin, A. 1988. Progress in understanding jointing over the past century. *GSA Bulletin*, **100**, 1181–1204, https://doi.org/10.1130/0016-7606(1988)100<1181:PIUJOT>2.3.CO;2

Reichenberger, V., Jakobs, H., Bastian, P. and Helmig, R. 2006. A mixed-dimensional finite volume method for two-phase flow in fractured porous media. *Advances in Water Resources*, **29**, 1020–1036, https://doi.org/10.1016/J.ADVWATRES.2005.09.001

Rizzo, R.E., Inskip, N.F. *et al.* 2024. Modelling geological CO_2 leakage: integrating fracture permeability and fault zone outcrop analysis. *International Journal of Greenhouse Gas Control*, **133**, 104105, https://doi.org/10.1016/J.IJGGC.2024.104105

Rogers, S., Enachescu, C., Trice, R. and Buer, K. 2007. Integrating discrete fracture network models and pressure transient data for testing conceptual fracture models of the Valhall chalk reservoir, Norwegian North Sea. *Geological Society, London, Special Publications*, **270**, 193–204, https://doi.org/10.1144/GSL.SP.2007.270.01.13

Rutqvist, J., Leung, C., Hoch, A., Wang, Y. and Wang, Z. 2013. Linked multicontinuum and crack tensor approach for modeling of coupled geomechanics, fluid flow and transport in fractured rock. *Journal of Rock Mechanics and Geotechnical Engineering*, **5**, 18–31, https://doi.org/10.1016/J.JRMGE.2012.08.001

Sævik, P.N. and Nixon, C.W. 2017. Inclusion of topological measurements into analytic estimates of effective permeability in fractured media. *Water Resources Research*, **53**, 9424–9443, https://doi.org/10.1002/2017WR020943

Sævik, P.N., Jakobsen, M., Lien, M. and Berre, I. 2014. Anisotropic effective conductivity in fractured rocks by explicit effective medium methods. *Geophysical Prospecting*, **62**, 1297–1314, https://doi.org/10.1111/1365-2478.12173

Snow, D.T. 1968. Rock fracture spacings, openings, and porosities. *Journal of the Soil Mechanics and Foundations Division*, **94**, 73–91, https://doi.org/10.1061/JSFEAQ.0001097

Srivastava, R.M., Frykman, P. and Jensen, M. 2005. *Geostatistical Simulation of Fracture Networks*. Springer, Dordrecht, https://doi.org/10.1007/978-1-4020-3610-1_30

Sun, J., Gamboa, E.S., Schechter, D. and Rui, Z. 2016. An integrated workflow for characterization and simulation of complex fracture networks utilizing microseismic and horizontal core data. *Journal of Natural Gas Science and Engineering*, **34**, 1347–1360, https://doi.org/10.1016/J.JNGSE.2016.08.024

Ţene, M., Bosma, S.B.M., Al Kobaisi, M.S. and Hajibeygi, H. 2017. Projection-based embedded discrete fracture model (pEDFM). *Advances in Water Resources*, **105**, 205–216, https://doi.org/10.1016/J.ADVWATRES.2017.05.009

Thomas, R.N., Paluszny, A. and Zimmerman, R.W. 2020. Growth of three-dimensional fractures, arrays, and networks in brittle rocks under tension and compression. *Computers and Geotechnics*, **121**, 103447, https://doi.org/10.1016/J.COMPGEO.2020.103447

Tran, M. and Jha, B. 2021. Effect of poroelastic coupling and fracture dynamics on solute transport and geomechanical stability. *Water Resources Research*, **57**, e2021WR029584, https://doi.org/10.1029/2021WR029584

Tran, N.H. 2007. Fracture orientation characterization: minimizing statistical modelling errors. *Computational Statistics & Data Analysis*, **51**, 3187–3196, https://doi.org/10.1016/J.CSDA.2006.10.024

Tsang, C.F., Neretnieks, I. and Tsang, Y. 2015. Hydrologic issues associated with nuclear waste repositories. *Water Resources Research*, **51**, 6923–6972, https://doi.org/10.1002/2015WR017641

Vermilye, J.M. and Scholz, C.H. 1995. Relation between vein length and aperture. *Journal of Structural Geology*, **17**, 423–434, https://doi.org/10.1016/0191-8141(94)00058-8

Vidal, J., Genter, A. and Chopin, F. 2017. Permeable fracture zones in the hard rocks of the geothermal reservoir at Rittershoffen, France. *Journal of Geophysical Research: Solid Earth*, **122**, 4864–4887, https://doi.org/10.1002/2017JB014331

Virtanen, P., Gommers, R. *et al.* 2020. SciPy 1.0: fundamental algorithms for scientific computing in Python. *Nature Methods*, **17**, 261–272, https://doi.org/10.1038/S41592-019-0686-2

Viswanathan, H.S., Ajo-Franklin, J. *et al.* 2022. From fluid flow to coupled processes in fractured rock: recent advances and new frontiers. *Reviews of Geophysics*, **60**, e2021RG000744, https://doi.org/10.1029/2021RG000744

Voskov, D., Saifullin, I. *et al.* 2024. open Delft Advanced Research Terra Simulator (open-DARTS). *Journal of Open Source Software*, **9**, 6737, https://doi.org/10.21105/joss.06737

Watkins, H., Bond, C.E., Healy, D. and Butler, R.W.H. 2015. Appraisal of fracture sampling methods and a new workflow to characterise heterogeneous fracture networks at outcrop. *Journal of Structural Geology*, **72**, 67–82, https://doi.org/10.1016/J.JSG.2015.02.001

Welch, M.J., Luthje, M. and Glad, A.C. 2019. Influence of fracture nucleation and propagation rates on fracture geometry: insights from geomechanical modelling. *Petroleum Geoscience*, **25**, 470–489, https://doi.org/10.1144/PETGEO2018-161

Welch, M.J., Lüthje, M. and Oldfield, S.J. 2020. *Modelling the Evolution of Natural Fracture Networks: Methods for Simulating the Nucleation, Propagation and Interaction of Layer-Bound Fractures*. Springer, https://doi.org/10.1007/978-3-030-52414-2

Wenli, Y., Sharifzadeh, M., Yang, Z., Xu, G. and Fang, Z. 2019. Assessment of fracture characteristics controlling fluid flow performance in discrete fracture networks (DFN). *Journal of Petroleum Science and Engineering*, **178**, 1104–1111, https://doi.org/doi: 10.1016/J.PETROL.2019.04.011

Wong, D.L.Y., Doster, F., Geiger, S. and Kamp, A. 2020. Partitioning thresholds in hybrid implicit-explicit representations of naturally fractured reservoirs. *Water Resources Research*, **56**, e2019WR025774, https://doi.org/10.1029/2019WR025774

Wong, D.L.Y., Doster, F. and Geiger, S. 2021. Embedded discrete fracture models. *In:* Lie, K.-A. and Møyner, O.E. (eds) *Advanced Modeling with the MATLAB Reservoir Simulation Toolbox*. Cambridge University Press, 375–408.

Zeeb, C., Gomez-Rivas, E., Bons, P.D. and Blum, P. 2013. Evaluation of sampling methods for fracture network characterization using outcrops. *AAPG Bulletin*, **97**, 1545–1566, https://doi.org/10.1306/02131312042

Zhang, Q., Wang, X., He, L. and Tian, L. 2021. Estimation of fracture orientation distributions from a sampling window based on geometric probabilistic method. *Rock Mechanics and Rock Engineering*, **54**, 3051–3075, https://doi.org/10.1007/S00603-021-02431-0

Zhang, W., Han, D., Jiao, K., Chen, Y., Yuan, Q., Gong, L. and Yu, B. 2024. Research on the THMC coupling model for enhanced geothermal systems based on the framework of EDFM. *Mechanisms and Machine Science*, **145**, 963–978, https://doi.org/10.1007/978-3-031-42987-3_67

Zimmerman, R.W. and Paluszny, A. 2023. *Fluid Flow in Fractured Rocks*. Wiley.